Surface Review and Letters, Vol. 6, Nos. 3 & 4 (1999) 411–433
© World Scientific Publishing Company

MANY-BODY EFFECTS AND THE METAL–INSULATOR TRANSITION AT SEMICONDUCTOR SURFACES AND INTERFACES

FERNANDO FLORES, JOSÉ ORTEGA and RUBÉN PÉREZ
Departamento de Física Teórica de la Materia Condensada,
Facultad de Ciencias, Universidad Autónoma de Madrid, Madrid 28049, Spain

Received 30 March 1999

The aim of this paper is to present a general perspective of the different correlation effects appearing at semiconductor surfaces and interfaces. The unifying theoretical picture is the generalized Hubbard Hamiltonian. In a first step, we show how such Hamiltonians can be analyzed using both a local density approach and many-body techniques. This discussion shows how to determine the different electron–electron interaction parameters appearing in the generalized Hubbard Hamiltonian, from a set of restricted LDA calculations for the full surface. Then, different surfaces and interfaces are analyzed; in particular, we consider the Si(111)-(7×7), -(5×5) and -(3×3) reconstructions as well as the Si-rich SiC(111)-($\sqrt{3}\times\sqrt{3}$) and -(3×3) surfaces. These Si-rich SiC(111) surfaces are shown to behave like a Mott–Hubbard insulator, while the Si(111) reconstructions are charge transfer systems presenting a variety of different behaviors; thus, the Si(111)-(7×7) is metallic, while the -(5×5) and the -(3×3) are found to be insulating. We have also analyzed the Sn/Ge(111)-(3×3) reconstruction, the alkali metal/GaAs(110) junction and the K/Si(111)-($\sqrt{3}\times\sqrt{3}$)-B interface. Our discussion shows that the alkali metal/GaAs and K/Si(111) interfaces present also a Mott–Hubbard metal–insulator transition, and that the Sn/Ge(111)-(3×3) interface is still metallic in spite of nonnegligible many-body effects appearing in the surface band density of states. We conclude that two-dimensional systems at semiconductor surfaces and interfaces present a rich variety of many-body effects that modify substantially the one-electron picture one gets from LDA calculations.

1. Introduction

Different theoretical and experimental evidences gathered recently for semiconductor surfaces and interfaces have shown the importance of electron correlation effects in these systems.[1–11] The metallization of very thin metal overlayers deposited on semiconductors was one of the first cases where these effects were recognized as critical for understanding the physics of the interface:[1] this problem is related to the formation of metal–semiconductor junctions in the early stages of the metal deposition on the semiconductor.[12,13] Following this line, the deposition of Sn or Pb on Ge(111) is also an example where electron correlation effects have been suggested[3] to play some role regarding, specifically, the formation of the Sn/Ge(111)-($\sqrt{3}\times\sqrt{3}$) or Pb/Ge(111)-($\sqrt{3}\times\sqrt{3}$) reconstructions; these systems present for not very low temperatures a surface phase transition[3,14] of the type $\sqrt{3}\times\sqrt{3}\to3\times3$, which might be coupled to those correlation effects.

On clean surfaces, different semiconductor reconstructions also show important many-body effects: the cases SiC(0001), SiC(111)-(3×3) and -($\sqrt{3}\times\sqrt{3}$), and Si(111)-(7×7) and -(5×5) are specific examples where different groups[4,7–11] have identified correlation effects that modify substantially the one-electron picture one can obtain from a local density (LD) calculation.

The aim of this paper is to present a general perspective of the different correlation effects appearing in the cases mentioned above. The unifying theoretical picture of this presentation is the generalized Hubbard Hamiltonian: we shall see how the examples mentioned above can be described by means of

the sort of Hamiltonian that includes, basically, local and nonlocal Coulomb interactions between the electrons of the system. In this picture, we shall discuss how the different examples analyzed in this paper can be classified into systems presenting correlation effects which are mainly associated with either *local* or *nonlocal* interactions. When these systems behave like insulators they correspond to what Zawasky and collaborators[15] have classified as either *Mott–Hubbard* or *charge transfer insulators*.

In Sec. 2 we present a theoretical discussion of how generalized Hubbard Hamiltonians can be analyzed within an LD approach and using many-body techniques. While most of the work in strongly correlated electrons has been devoted to idealized models, our aim is to study the effect of the electron–electron interaction in the band structure of the surface or interface between real materials. The LD approach in terms of localized orbitals discussed in Subsec. 2.1 proves fundamental in the accurate mapping of the band structure into the generalized Hubbard Hamiltonian. In particular, it provides a way of determining the electron–electron interaction parameters [U and J; see the Hamiltonian (1) below] appearing in the generalized Hubbard Hamiltonian for the surface states we want to analyze, from a set of LDA calculations for the full surface. Our treatment of the many-body problem introduces dynamical effects associated with the correlation by the use of a self-energy, and is presented in Subsec. 2.2. Notice that various schemes, like the "LDA + U"[16] or the self-interaction correction (SIC) method,[17] have been proposed to include electron–electron interactions in LDA calculations. Although these schemes lead to significant improvements, they do not capture the dynamical effects included by the self-energy approach. The discussion in Sec. 2 is presented as an introduction to the more specific analysis of different semiconductor surfaces and interfaces that will be discussed in Secs. 3 and 4. Readers not specifically interested in the theory presented in Sec. 2 can proceed directly to Secs. 3 and 4.

2. Generalized Hubbard Hamiltonians; Metal–Insulator Transitions

In this section, we present the basic theoretical approach that has been used by many different researchers[18] in order to understand the electron correlation effects associated with an electron gas; our presentation always keeps in mind the particular two-dimensional cases appearing at semiconductor surfaces or interfaces.

Our starting point is the generalized Hubbard Hamiltonian

$$\hat{H} = \sum_{\alpha,\sigma} E_\alpha \hat{n}_{\alpha\sigma} + \sum_{\alpha\neq\beta,\sigma} t_{\alpha\beta}\hat{c}^\dagger_{\alpha\sigma}\hat{c}_{\beta\sigma} + \sum_{\alpha} U_\alpha \hat{n}_{\alpha\uparrow}\hat{n}_{\alpha\downarrow} + \frac{1}{2}\sum_{\alpha\neq\beta,\,\sigma\sigma'} J_{\alpha\beta}\hat{n}_{\alpha\sigma}\hat{n}_{\beta\sigma'}\,, \tag{1}$$

where E_α is the energy level of the wave function associated with orbital α; $t_{\alpha\beta}$ defines the effective hopping between orbitals α and β; and U_α and $J_{\alpha\beta}$ are the on-site (α α) and off-site (α β) Coulomb interactions. We assume that there is only one orbital per site. In Eq. (1), $\hat{n}_{\alpha\sigma}$, $\hat{c}^\dagger_{\alpha\sigma}$ and $\hat{c}_{\beta\sigma}$ are the occupation number, and creation and anhiliation operators, respectively.

The Hamiltonian (1) has been used as the basic approach to analyze many different correlation problems not limited to the surface or interface cases discussed in this paper. Let us note that the restricted Hubbard Hamiltonian is obtained by taking $J_{\alpha\beta} = 0$ in the Hamiltonian (1); the interest in using this restricted case appears when one considers a half-filled band — a problem for which, as discussed below, the general Hamiltonian (1) can be reduced to this limit. Although most of the work on electron correlation effects and the metal–insulator transition has focused on the solution of this restricted Hubbard Hamiltonian, many of the surface and interface systems we will consider below present bands with filling factors different from one-half. In these cases, the off-site Coulomb interaction $J_{\alpha\beta}$ included in the generalized Hubbard Hamiltonian plays a crucial role in driving the metal–insulator transition.

In Subsec. 2.1 we present the LD solution of the generalized Hubbard Hamiltonian (1), obtained using the dynamical mean field (DMF) approximation.[19] In this approximation, which can be considered as the exact solution in the limit of an infinite coordination number, the effects of the off-site Coulomb interaction, $J_{\alpha\beta}$, are treated in a mean field approximation, and the correlation effects associated with U_α can be analyzed in a

local way, neglecting any interference between different sites (say, α and β). The second part of this section (Subsec. 2.2) is devoted to explaining the self-energy approach to the calculation of the density of states. This approach provides a general procedure for analyzing the metal–insulator transition in systems described by the Hamiltonian (1). In some specific cases, easier ways to study the correlated density of states can be devised; some examples will be discussed in Sec. 3.

2.1. *LD solution of the generalized Hubbard Hamiltonian in the DMF limit*

Following an LD approach, the total energy, E, of the system described by the Hamiltonian (1) can be shown[20] to be a *function* of the orbital occupation numbers, $n_{\alpha\sigma} = \langle \hat{n}_{\alpha\sigma} \rangle$ ($\langle\rangle$ indicates the expectation value on the ground state):

$$E \equiv E(n_{1\uparrow}, n_{1\downarrow}, \ldots, n_{\alpha\sigma}, \ldots) = E(\{n_{\alpha\sigma}\}) \,. \quad (2)$$

As with standard density functional theory, the ground state orbital occupation numbers are the set $\{n_{\alpha\sigma}\}$, which minimizes $E(\{n_{\alpha\sigma}\})$; this minimization process is equivalent to the self-consistent solution of an effective one-electron Hamiltonian, $\hat{H}^{\text{eff}}$, which also depends on these occupation numbers. In what follows, we show how $\hat{H}^{\text{eff}}$ can be defined, using the DMF approximation, in terms of the parameters of the Hamiltonian (1) and the orbital occupation numbers.

As the starting point, it is useful to split the total energy into the kinetic, T, and many-body, E^{mb}, contributions,

$$E = T(\{n_{\alpha\sigma}\}) + E^{\text{mb}}(\{n_{\alpha\sigma}\}) \,, \quad (3)$$

in such a way that, following Kohn and Sham, we can introduce the following effective Hamiltonian:[20]

$$\hat{H}^{\text{eff}} = \sum_{\alpha,\sigma} (E_\alpha + V^{\text{mb}}_{\alpha\sigma}) \hat{n}_{\alpha\sigma} + \sum_{\alpha\neq\beta,\sigma} t_{\alpha\beta} \hat{c}^\dagger_{\alpha\sigma} \hat{c}_{\beta\sigma} \,, \quad (4)$$

where

$$V^{\text{mb}}_{\alpha\sigma} = \frac{\partial E^{\text{mb}}}{\partial n_{\alpha\sigma}} \,. \quad (5)$$

Solving Eqs. (4) and (5) self-consistently we can calculate the $\{n_{\alpha\sigma}\}$ of the ground state, and using Eq. (2) we obtain the total energy of the system.

Obviously, the main problem in this approach is to determine E^{mb} in Eq. (3) as a function of the orbital occupation numbers. Again, it is convenient to split this term in the so-called Hartree, exchange and correlation contributions. While it is quite straightforward to write down the functional dependence of the Hartree term, exchange and correlation are more involved, and the DMF limit will be explicitly used to get a closed expression in terms of the orbital occupation numbers.

From Eq. (1), we see that the Hartree contribution is given by

$$E^H(\{n_{\alpha\sigma}\}) = \sum_\alpha U_\alpha n_{\alpha\uparrow} n_{\alpha\downarrow} + \frac{1}{2} \sum_{\alpha\neq\beta,\,\sigma\sigma'} J_{\alpha\beta} n_{\alpha\sigma} n_{\beta\sigma'} \,, \quad (6)$$

while the exchange contribution is

$$E^x(\{n_{\alpha\sigma}\}) = -\frac{1}{2} \sum_{\alpha\neq\beta,\sigma} J_{\alpha\beta} n_{\alpha\beta\sigma} n_{\beta\alpha\sigma} \,, \quad (7)$$

with $n_{\alpha\beta\sigma} = \langle \hat{c}^\dagger_{\alpha\sigma} \hat{c}_{\beta\sigma} \rangle$. We can make use of the sum rule[20]

$$\sum_{\beta\neq(\alpha)} n_{\alpha\beta\sigma} n_{\beta\alpha\sigma} = n_{\alpha\sigma}(1 - n_{\alpha\sigma}) \quad (8)$$

to write

$$E^x(\{n_{\alpha\sigma}\}) = -\frac{1}{2} \sum_{\alpha,\sigma} J_\alpha n_{\alpha\sigma}(1 - n_{\alpha\sigma}) \,, \quad (9)$$

which yields the exchange energy as the interaction, J_α, between $n_{\alpha\sigma}$ and its hole, $1 - n_{\alpha\sigma}$. In the DMF approximation, the hole is located in the nearest neighbors (nn) of the α site, and J_α in Eq. (9) represents the interaction between nn electrons.

The correlation contribution to the energy, in the DMF approximation, is a local property that can be shown[20] to depend on $n_{\alpha\sigma}$ as follows:

$$E^c(\{n_{\alpha\sigma}\}) = -\frac{1}{2} \sum_{\alpha,\sigma} f_{\alpha\sigma}(U_\alpha - J_\alpha) n_{\alpha\sigma}(1 - n_{\alpha\sigma}) \,. \quad (10)$$

This equation yields the correlation energy as the Coulomb interaction between the charge $n_{\alpha\sigma}$ and its

correlation hole $f_{\alpha\sigma}(1-n_{\alpha\sigma})$. This hole is located inside the α site, and reduces the exchange hole from $1-n_{\alpha\sigma}$ to $(1-f_{\alpha\sigma})(1-n_{\alpha\sigma})$: this is the reason for having $U_\alpha - J_\alpha$ instead of U_α in Eq. (10). Values of $f_{\alpha\sigma}$ as a function of $n_{\alpha\sigma}$ are given in Ref. 20 for different $(U_\alpha - J_\alpha)/t$ values.

Equations (6), (9) and (10) define the many-body energy,

$$E^{\rm mb}(\{n_{\alpha\sigma}\}) = E^H(\{n_{\alpha\sigma}\}) + E^x(\{n_{\alpha\sigma}\}) + E^c(\{n_{\alpha\sigma}\})\,, \quad (11)$$

and the many-body potential, $V^{\rm mb}_{\alpha\sigma}$, in Eq. (5), as

$$\begin{aligned} V^{\rm mb}_{\alpha\sigma} &= \frac{\partial E^H}{\partial n_{\alpha\sigma}} + \frac{\partial E^x}{\partial n_{\alpha\sigma}} + \frac{\partial E^c}{\partial n_{\alpha\sigma}} \\ &= U_\alpha n_{\alpha\bar\sigma} + \sum_{\beta\neq(\alpha)} J_{\alpha\beta} n_\beta - J_\alpha\left(\frac{1}{2} - n_{\alpha\sigma}\right) \\ &\quad - f_{\alpha\sigma}(U_\alpha - J_\alpha)\left(\frac{1}{2} - n_{\alpha\sigma}\right)\,, \end{aligned} \quad (12)$$

where $n_\beta = n_{\beta\uparrow} + n_{\beta\downarrow}$, and $f_{\alpha\sigma}$ has been assumed, for the sake of simplicity, to be practically constant.

Equations (4) and (12) define our effective one-electron Hamiltonian associated with Eqs. (1). This is an important result from both the conceptual and the applied point of view. It makes it possible to discuss the equivalence of different simplified Hubbard Hamiltonians under particular physical conditions, as will be shown below. On the other hand, it is extremely relevant from the point of view of realistic applications, because it provides a direct link between the accurate one-electron LDA calculations for surface or interface problems and the many-body Hamiltonian (1) we want to use to include correlation effects.

The starting point for calculating the parameters of the Hamiltonian (1) is the fitting of the relevant surface bands in our ground state calculation to the one-electron Hamiltonian defined in Eq. (4). This first step provides the hopping parameters, $t_{\alpha\beta}$, and on-site effective levels, $E_\alpha + V^{\rm mb}_{\alpha\sigma}$, where electron–electron contributions (U_α, $J_{\alpha\beta}$) are included with the ground state occupation numbers. The sole analysis of the ground state bands is clearly not enough to determine the individual contributions to the effective levels, but the analysis of the surface bands from different "restricted LDA calculations"[6] using Eq. (12) provides a way to calculate E_α, U_α, J_α and $J_{\alpha\beta}$. In this approach, the filling factors of the different surface bands are varied and the corresponding occupation numbers, $n_{\alpha\sigma}$, are changed. LDA self-consistency for the new restricted case (where the filling factors are kept fixed) yields, in its turn, new parameters $E_\alpha + V^{\rm mb}_\alpha$, related to the new occupation numbers, $\{n_{\beta\sigma}\}$. The application of Eq. (12), with the appropriate V^x and V^c, which defines how $V^{\rm mb}_\alpha$ depends on $\{n_{\beta\sigma}\}$, to the different restricted LDA calculations provides a set of equations that would allow one, in principle, to calculate E_α, U_α, J_α and $J_{\alpha\beta}$. One should note, however, that not all the parameters, U_α and $J_{\alpha\beta}$, can be determined by this procedure. There is always, at least, one parameter that still remains undetermined by the set of equations (12). We will usually choose to obtain $J_{\alpha\beta}$ by means of an independent electrostatic model (see Sec. 3 for details). We must stress that, in order to accurately complete this program, one has to introduce the exchange and correlation contributions; otherwise, one would only use the Hartree potential and the fitting is liable to yield inaccurate parameters.

The results obtained above for the many-body potential, $V^{\rm mb}_{\alpha\sigma}$, allow us also to analyze the equivalence of different Hubbard Hamiltonians, depending on the physical conditions of the problem. Consider, as a first example, the case of a lattice with equivalent sites and having one electron per site (the half-filled band case). This is a typical problem that has been usually analyzed by considering a restricted Hamiltonian with an effective on-site interaction, $U^{\rm eff}$. How to establish contact between the two models? In this particular case, we look for solutions such that $n_{\alpha\uparrow} + n_{\alpha\downarrow} = 1$, namely with electrons fluctuating at each site between spins up and down (in the insulating phase, electrons are localized one per site, with their spins up or down). For the general Hamiltonian, the local potential, $V^{\rm mb}_{\alpha\sigma}$, would change with $n_{\alpha\sigma}$ as follows:

$$\delta V^{\rm mb}_{\alpha\sigma} = [U_\alpha - J_\alpha - f_{\alpha\sigma}(U_\alpha - J_\alpha)]\delta n_{\alpha\bar\sigma} \quad (13)$$

(since $\delta n_{\alpha\sigma} = -\delta n_{\alpha\bar\sigma}$), while for the restricted Hamiltonian,

$$\delta V^{\rm mb}_{\alpha\sigma} = (U^{\rm eff}_\alpha - f_{\alpha\sigma} U^{\rm eff}_\alpha)\delta n_{\alpha\bar\sigma}\,. \quad (14)$$

A comparison of Eqs. (13) and (14) yields

$$U^{\rm eff}_\alpha = U_\alpha - J_\alpha\,, \quad (15)$$

defining the effective intrasite interaction as the difference between U_α and the nn Coulomb interaction, J_α.

In the second example, we consider also a lattice with all the sites equivalent but having only *one* electron every *two* sites. This is the so called one-fourth filling band case. For this particular case, the metal–insulator transition cannot usually be driven by the on-site Coulomb interaction U; in particular, this phase transition is associated with electron fluctuations between two sites (in the insulating phase, there is one electron in each occupied site, and half of the lattice sites are empty). This problem has usually been analyzed by means of a generalized Hubbard Hamiltonian reading

$$\hat{H} = \sum_{\alpha,\sigma} E_\alpha \hat{n}_{\alpha\sigma} + \sum_{\alpha\neq\beta,\,\sigma} t_{\alpha\beta}\hat{c}^\dagger_{\alpha\sigma}\hat{c}_{\beta\sigma} + U^{\text{eff}} \sum_{\alpha} \hat{n}_{\alpha\uparrow}\hat{n}_{\alpha\downarrow} + \frac{1}{2} J^{\text{eff}} \sum_{\text{nn}} \hat{n}_\alpha \hat{n}_\beta \,, \quad (16)$$

where only the nn interaction, J^{eff}, is introduced. This effective off-site interaction is expected to drive the metal–insulator transition. In order to establish the equivalence between Hamiltonians (1) and (16) (for the one-fourth filling band case), we note that one is only interested in fluctuations such that $n_1 + n_2 = 1$, where n_1 and n_2 are the charges (summed over the spin) of the inequivalent sites 1 and 2. In the complete Hubbard Hamiltonian,

$$\delta V^{\text{mb}}_{1\uparrow} = [U - J - f_{1\uparrow}(U-J)]\delta n_{1\downarrow} + \sum_{\beta\neq 1} J_{1\beta}\delta n_\beta - J\delta n_2 - f_{1\uparrow}(U-J)\delta n_2 \,, \quad (17)$$

where use of $\delta n_1 + \delta n_2 = 0$ has been made, and J represents the nn Coulomb interaction. A similar equation for site 2 can be written.

For the Hamiltonian (16), the many-body potential, $V^{\text{mb}}_{1\uparrow}$, is related to changes in the charges by the equation

$$\delta V^{\text{mb}}_{1\uparrow} = [U^{\text{eff}} - J^{\text{eff}} - f_{1\uparrow}(U^{\text{eff}} - J^{\text{eff}})]\delta n_{1\downarrow} + \sum_{\text{nn}} J^{\text{eff}}\delta n_\beta - J^{\text{eff}}\delta n_2 - f_{1\uparrow}(U^{\text{eff}} - J^{\text{eff}})\delta n_2 \,. \quad (18)$$

Comparison of Eqs. (17) and (18) yields the following equivalence between the Hamiltonians (1) and (16):

$$U - J = U^{\text{eff}} - J^{\text{eff}} \,, \quad (19)$$

$$\left(\sum_{\beta\neq 1} J_{1\beta}\right)^{\text{Madel.}} - J = \left(\sum_{\text{nn}} J^{\text{eff}}\right) - J^{\text{eff}} \,. \quad (20)$$

In this equation $(\sum_{\beta\neq 1} J_{1\beta})^{\text{Madel.}}$ is the Madelung potential, $(1+\gamma)J$, created by the charges $n_2 = 1$ and $n_1 = -1$ on the lattice sites 2 and 1, respectively. For a lattice coordination Z, the second equation yields

$$\gamma J = (Z-1)J^{\text{eff}} \,. \quad (21)$$

Equations (19) and (21) define the effective parameters of the Hamiltonian (16) in terms of the quantities appearing in the Hamiltonian (1). Notice that in this equivalence, J^{eff} is defined by the Madelung potential, the lattice coordination Z and the nn interaction, J. On the other hand, the new value of U is defined by Eq. (19), which tells us that the difference between U and the nn interaction, J, is the same in the two Hamiltonians.

2.2. *Density of states; self-energies and the metal–insulator transition*

The LD solution presented above gives the orbital occupancies, $\{n_{\alpha\sigma}\}$, and the total energy of the system, but does not provide a good solution for its density of states. Only for systems having small correlation effects can we expect the effective Hamiltonian (4) to adequately yield their density of states. In particular, the metal–insulator transition of Hamiltonian (1) has to be analyzed introducing other techniques.

A good solution to this problem is provided by the use of many-body techniques.[21,22] This approach can be related to the LD solution of Subsec. 2.1 in the following way. First of all, notice that the many-body potential, $V^{\text{mb}}_{\alpha\sigma}$ [Eq. (12)], includes three contributions — the Hartree, the exchange and the correlation terms. Within the DMF approximation, the Hartree and the exchange potentials are well described by the LD contributions; then, in order to have a good description of the density of states, we only have to introduce dynamical effects associated with correlation. This amounts to replacing

$V^c(\{n_{\alpha\sigma}\})$ by an appropriate self-energy, $\Sigma^c(\{n_{\alpha\sigma}\})$; the knowledge of this quantity allows us to define the local density of states, $\rho_{\alpha\sigma}(w)$, as follows:

$$\rho_{\alpha\sigma}(w) = -\frac{1}{\pi}\,\mathrm{Im}\{G_{\alpha\alpha,\sigma}(w)\}\,,$$
$$n_{\alpha\sigma} = \int_{-\infty}^{E_F} dw\rho_{\alpha\sigma}(w)\,, \tag{22}$$

where $G_{\alpha\alpha,\sigma}(w)$ is the $(\alpha\alpha,\,\sigma)$ component of the Green function defined by the matrix

$$\mathbf{G}(w) = [w\mathbf{I} - \mathbf{H}]^{-1} \tag{23}$$

where

$$H_{\alpha\alpha,\sigma} = E_\alpha + V^H_{\alpha\sigma} + V^x_{\alpha\sigma} + \Sigma^c_{\alpha\sigma}(w) \tag{24}$$

and

$$H_{\alpha\beta,\sigma} = t_{\alpha\beta}\,. \tag{25}$$

The main problem in this approach is to calculate $\Sigma^c_{\alpha\sigma}(w)$. Many different approximations have been proposed. In the simplest approach, using a second order perturbation theory, $\Sigma^c_{\alpha\sigma}(w)$ is approximated[23] by

$$\Sigma^{c(2)}_{\alpha\sigma}(w) = U^2\int_{-\infty}^{\infty} d\varepsilon_1 d\varepsilon_2 d\varepsilon_3\frac{\tilde\rho_{\alpha\sigma}(\varepsilon_1)\tilde\rho_{\alpha\bar\sigma}(\varepsilon_2)\tilde\rho_{\alpha\bar\sigma}(\varepsilon_3)}{w+\varepsilon_2-\varepsilon_1-\varepsilon_3+i0^+}$$
$$\times\,[f_1f_3(1-f_2)-(1-f_1)(1-f_3)f_2]\,, \tag{26}$$

where $f_i = f(\varepsilon_i)$ denotes the Fermi distribution and $\tilde\rho_{\alpha\sigma}(\varepsilon_i)$ is the local density of states as calculated from the one-electron LD approximation discussed above.

A much better approximation is obtained by realizing that (i) $\Sigma^{c(2)}_{\alpha\sigma}(w)$ goes to

$$U^2\,\frac{n_{\alpha\bar\sigma}(1-n_{\alpha\bar\sigma})}{w-(E_\alpha+V^H_\alpha+V^x_\alpha+V^c_\alpha)} \tag{27}$$

for $w\to\infty$, $n_{\alpha\bar\sigma}$ being the charges calculated in LD, and (ii) the atomic limit of $\Sigma^c_{\alpha\sigma}(w)$,

$$\Sigma^{c,\mathrm{at}}_{\alpha\sigma}(w) = \frac{U^2 n_{\alpha\bar\sigma}(1-n_{\alpha\bar\sigma})}{w-(E_\alpha+V^H_\alpha+V^x_\alpha+V^c_\alpha)-(1-2n_{\alpha\bar\sigma})U}\,, \tag{28}$$

also goes to the same limit for $U\to 0$. This suggests to define the following interpolative self-energy:[24]

$$\Sigma^c_{\alpha\sigma}(w) = \frac{\Sigma^{c(2)}_{\alpha\sigma}(w)}{1-a\Sigma^{c(2)}_{\alpha\sigma}(w)}\,, \tag{29}$$

with

$$a = \frac{(1-2n_{\alpha\bar\sigma})U}{U^2 n_{\alpha\bar\sigma}(1-n_{\alpha\bar\sigma})}\,. \tag{30}$$

It is easy to check that in the limit $U/t\to 0$, $a\Sigma^{c(2)}_{\alpha\sigma}$ goes to zero and $\Sigma^c_{\alpha\sigma}$ goes to $\Sigma^{c(2)}_{\alpha\sigma}$. On the other hand, for $U/t\to\infty$, $\Sigma^{c(2)}_{\alpha\sigma}$ goes to

$$U^2\,\frac{n_{\alpha\bar\sigma}(1-n_{\alpha\bar\sigma})}{w-(E_\alpha+V^H_\alpha+V^x_\alpha+V^c_\alpha)} \tag{31}$$

and Eq. (29) recovers the atomic limit. Accordingly, the self-energy defined by Eq. (29) yields both the small and the high U limit, and has been checked in different calculations to be a fair approximation to $\Sigma^c_{\alpha\sigma}$.[25]

A final step in this evolution was given by Rozenberg *et al.*,[26] who proposed calculating $\Sigma^{c(2)}_{\alpha\sigma}$ by using for $\tilde\rho_{\alpha\sigma}(w)$ the local density of states obtained by replacing $V^c_{\beta\sigma}$ with $\Sigma^c_{\beta\sigma}(w)$ in all sites save the same place α, where we want to calculate $\tilde\rho_{\alpha\sigma}(w)$. In this way, the zeroth order density of states, used to calculate $\Sigma^{c(2)}_{\alpha\sigma}$ and $\Sigma^c_{\alpha\sigma}$, includes all the correlation effects associated with other sites. We stress that defining $\tilde\rho_{\alpha\sigma}(w)$ by replacing $V^c_{\beta\sigma}$ with $\Sigma^c_{\beta\sigma}(w)$ in all sites, including α, has been checked to yield much worse results than the previous ansatz.[27] Notice also that in the proposal of Rozenberg *et al.*,[26] $\Sigma^c_{\beta\sigma}(w)$ has to be calculated self-consistently, because $\tilde\rho_{\alpha\sigma}(w)$, defining $\Sigma^{c(2)}_{\alpha\sigma}$, depends itself on the self-energy. These authors have shown that this procedure yields for a Hubbard Hamiltonian solutions, within the DMF approximation, that provide good estimates for the metal–insulator transition.

As an example of the results given by this approach, Fig. 1 shows the density of states calculated for a half-filled rectangular lattice,[28] using a restricted Hubbard Hamiltonian ($J_{\alpha\beta} = 0$). Different curves correspond to different values of U^{eff}/W (W is the bandwidth). These results show the typical evolution of the density of states of this case when U^{eff}/W varies from 0 to ∞. Initially ($U^{\mathrm{eff}}/W\to 0$), the system shows a free electron density of states; when U^{eff}/W increases, two peaks associated with E_0 and E_0+U^{eff}, the ionization and the affinity levels of the single site, start to evolve and a Kondo-like peak

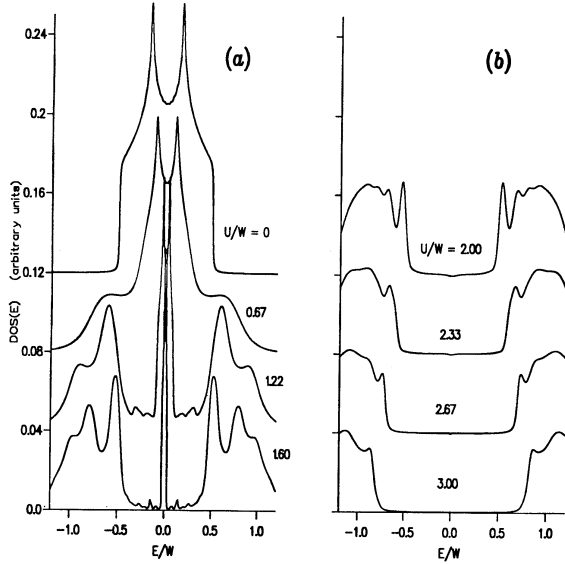

Fig. 1. Local density of states for a restricted Hubbard Hamiltonian of a two-dimensional rectangular lattice. Different curves correspond to different values of U^{eff}/W (see text for details).

appears at the Fermi energy. Eventually, the insulating phase is found (in Fig. 1 for $U^{\text{eff}}/W > 1.6$), and the density of states shows two peaks at E_0 and $E_0 + U^{\text{eff}}$, each having a width of $\sim W/2$. Then, the metal–insulator transition appears for $U^{\text{eff}}/W \simeq 1.6$, with U^{eff} defined by $U^{\text{eff}} = U_\alpha - J_\alpha$, as discussed above.

The case of a band filling different from one-half has to be analyzed using either the generalized Hubbard Hamiltonian (1) or another one, such as the Hamiltonian (16), which has been shown to be equivalent to it. In order to keep the discussion simple, we consider only the quarter-filling band case, which is well described by the Hamiltonian (16), and instead of considering its general solution, we discuss the limit $U^{\text{eff}}/W \gg 1$, and analyze its possible metal–insulator transition as a function of J^{eff}.[22]

To start, consider the exchange and correlation energies in the limit $U^{\text{eff}}/W \to \infty$. From Eqs. (9) and (10) we see that for $f_{\alpha\sigma} \to 1$, as corresponds to the case $U^{\text{eff}}/W \to \infty$,

$$E^x + E^c = -\frac{1}{2}\sum_{\alpha\sigma} U^{\text{eff}} n_{\alpha\sigma}(1 - n_{\alpha\sigma}) \qquad (f_{\alpha\sigma} = 1)\,; \qquad (32)$$

in this case $n_{\alpha\sigma} + n_{\alpha\bar{\sigma}}$ is either 1 or 0 and one can check that this energy cancels out exactly the Hartree energy associated with the intra-atomic Coulomb interaction. This shows that the total energy of the system in this limit, $U^{\text{eff}} \to \infty$, is given by

$$E(\{n_{\alpha\sigma}\}) = T(\{n_{\alpha\sigma}\}) + E^H_{\text{inter}}(\{n_{\alpha\sigma}\})\,, \qquad (33)$$

where $E^H_{\text{inter}}(\{n_{\alpha\sigma}\})$ is the Hartree energy associated with the interaction between charges in different sites.

The metal–insulator transition can be analyzed by comparing the energies of the two phases: in the metallic phase, the total energy is given only by the kinetic term, a contribution that, per electron, is well approximated by $-W/4$ (W being the bandwidth); in the insulating phase, the intersite Coulomb interaction per electron is due to the rearrangement of the mean charge, $-ZJ^{\text{eff}}/4$, with Z the lattice coordination. Comparison between these values show that the metal–insulator transition should appear for $J^{\text{eff}} \simeq W/Z$.

Detailed calculations using the self-energy approach confirm this picture.[22] Figure 2 shows a scheme of the local density of states found for this problem, as a function of J^{eff}/W: (i) for $J^{\text{eff}}/W \ll 1/Z$, we have the metallic phase, with local densities of states showing around E_F, because of the high U^{eff} value, bands having a weight of only three-quarters of the electron; (ii) for $J^{\text{eff}}/W \gg 1/Z$, we recover the insulating phase with a broken symmetry, the site a allocating one electron and site b being empty; (iii) at intermediate values of J^{eff} ($J^{\text{eff}}/W \simeq 1/Z$), we find a Kondo-like peak at the Fermi energy, and a density of states at sites a and b resembling the insulating phase.

Furthermore, it is interesting to note that these results, for $U/t \to \infty$ and a quarter-filling, can also be recovered using a spinless Hamiltonian. In this limit, $U/t \to \infty$, only one electron can fill a site: this suggests using a spinless Hamiltonian, whose solution automatically includes exchange effects that forbid two electrons to occupy simultaneously a single site. This Hamiltonian reads

$$\hat{H}^{\text{spinless}} = \sum_\alpha E_\alpha \hat{n}_\alpha + \sum_{\alpha\neq\beta} t_{\alpha\beta}\hat{c}^\dagger_\alpha \hat{c}_\beta + \frac{1}{2}\sum_{\alpha\neq\beta} J_{\alpha\beta}\hat{n}_\alpha \hat{n}_\beta\,. \qquad (34)$$

The use of a mean field approximation for the Coulomb term $J_{\alpha\beta}\hat{n}_\alpha\hat{n}_\beta$ allows us to analyze in a

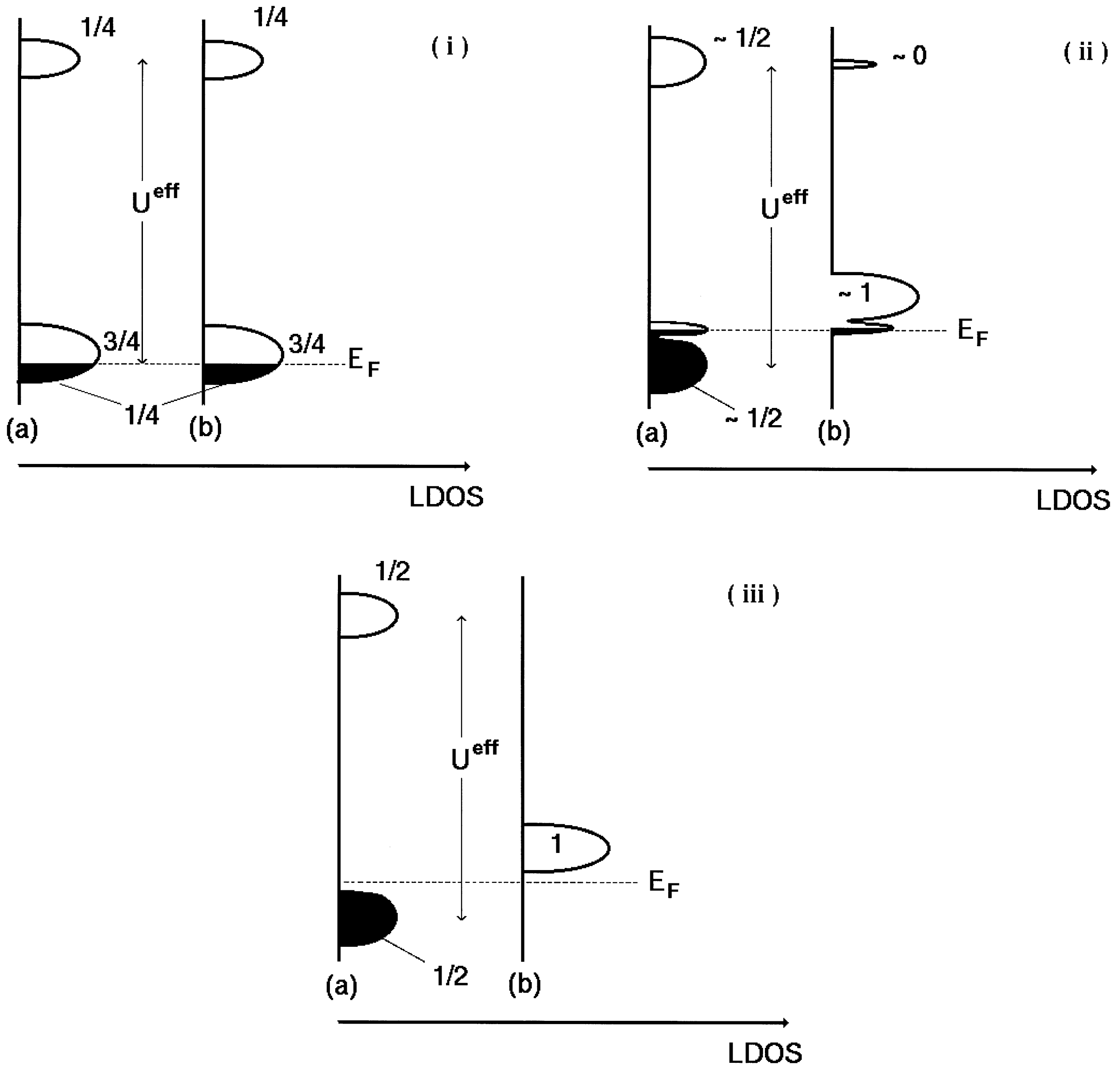

Fig. 2. Scheme showing the local density of states on the different sites (a) and (b) of a two-dimensional Hubbard Hamiltonian, for $U^{\text{eff}} \gg W$ (see text), and a quarter band filling. (i) For $J^{\text{eff}}/W \ll 1/Z$, one finds a metallic phase; the weight of this density of states around E_F is 3/4 (per spin). (ii) For $J^{\text{eff}}/W \sim 1/Z$, a Kondo-like peak appears at the Fermi energy; moreover, sites (a) and (b) have a different density of states, resembling the insulator phase. (iii) For $J^{\text{eff}}/W \gg 1/Z$, the insulating phase appears with an empty density of states in site (b), and a half-filled density of states in site (a).

simple way the metal–insulator transition associated with $J_{\alpha\beta}$ in this spinless Hamiltonian. In particular, the condition found above, $J^{\text{eff}} \simeq W/Z$, can be retrieved from this mean field solution.

A word of caution is in order here. The point to realize is that the Hamiltonian (34) yields a total local DOS of one electron per site (spin is not included in that Hamiltonian); although this provides a reasonable solution for the occupied part of the spectrum, the empty part is not well represented by that DOS. The reason is that in the empty sites we can inject one electron with spin up or down: this suggests that, in the solution to the Hamiltonian (34), the empty DOS should be multiplied by 2. Then,

the DOS calculated in this way yields a reasonable description of the results shown in Fig. 2.

3. Surfaces

3.1. *Si(111)-(7 × 7), -(5 × 5) and -(3 × 3) reconstructions*

The Si(111)-(7 × 7) surface[29] has probably been the most extensively studied semiconductor surface. This and other similar $(2n+1) \times (2n+1)$ reconstructions[31] are currently accepted to follow the dimer–adatom–stacking fault (DAS) model.[32,42] Figures 3 and 4 show the geometries of the 5 × 5 and 7 × 7 respectively. In this section we present a theoretical analysis of the electron correlation effects associated with the surface bands appearing in those three different reconstructions. Firstly, we discuss the global electronic properties of these surfaces using LD calculations. In particular, we determine the filling factors of the relevant bands and the parameters of the corresponding generalized Hubbard Hamiltonian for the different reconstructions. Then, we proceed to analyze the properties of the 2D electron gas localized in each surface.

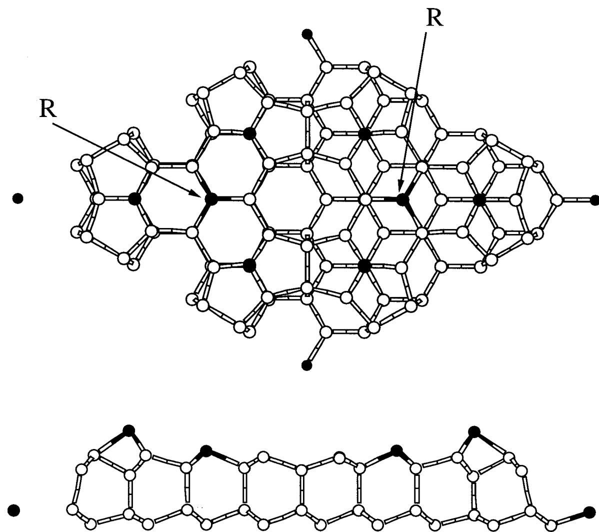

Fig. 3. Unit cell of the Si(111)-(5 × 5) reconstruction: top view and side view. Surface atoms with dangling bonds are marked with black circles: the corner hole (the atom at the corner of the unit cell), the two rest atoms (labeled R), and the six adatoms, protruding from the surface.

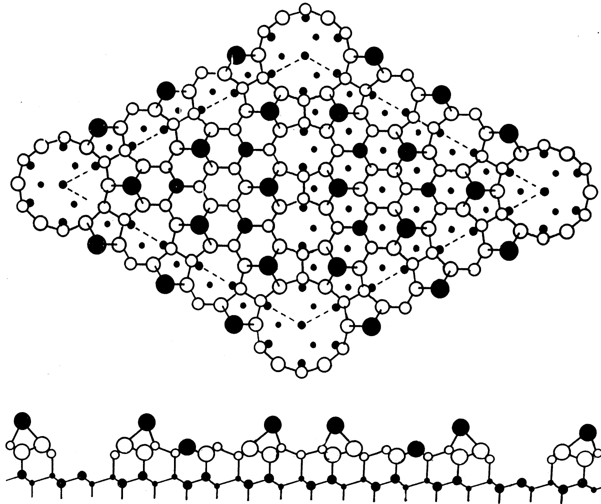

Fig. 4. Unit cell of the Si(111)-(7 × 7) reconstruction: top view and side view. In the top view, the adatoms are represented by the largest black dots and the rest atoms by the second-largest black dots. The corner hole atom is the one at the corner of the unit cell.

3.1.1. *Local density calculations; surface bands and Hubbard Hamiltonian*

We start our study with the Si(111)-(7 × 7) surface. Figure 5 shows the LDA surface bands corresponding to this reconstruction. These bands, and the relaxed ionic geometry of minimum energy, have been calculated using a self-consistent local orbital method.[33] We have checked in the easier-to-handle Si(111)-(5×5) reconstruction that this method yields results similar to the ones obtained using standard plane wave LDA calculations.[34] The surface bands of the Si(111)-(7 × 7) reconstruction show a bunch of 12 bands located around the Fermi energy, E_f, an independent band ≈ 0.55 eV below E_f and six surface bands ≈0.8 eV below E_f. These bands are related to the different dangling bonds of the 7 × 7 surface; in particular, the six bands located ≈0.8 eV below E_f are associated with the six rest atoms (see Fig. 4), the single band with the corner hole, and the 12 bands around E_f with the 12 adatoms.[35,36] Note that the position of the corner hole band in all the DAS reconstructions is very much dependent on allowing the corner atom to relax towards the vacuum side: a calculation with a small number of layers in the surface slab, where the neighbors of the corner hole have to be kept fixed, notably restricts that relaxation and yields a band much closer to the ones associated with the adatoms.[37]

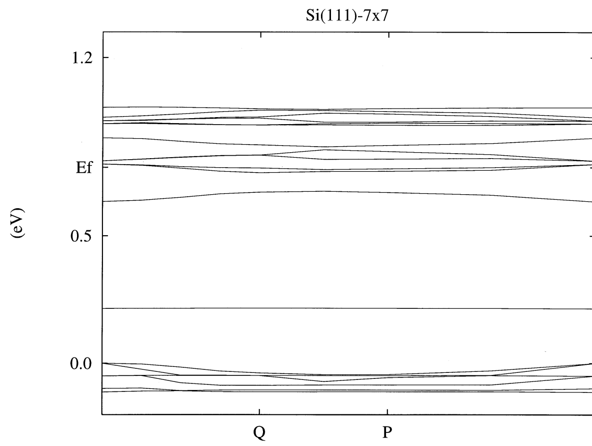

(a)

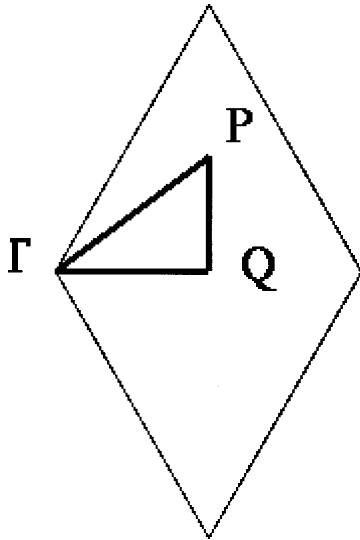

(b)

Fig. 5. (a) LDA surface bands corresponding to the Si(111)-(7 × 7) reconstruction. The 12 bands around E_F are essentially derived from the 12 adatom dangling bonds, the band ∼0.55 eV below E_F is related to the corner hole atom dangling bond, and the 6 bands ∼0.8 eV below E_F are associated with the 6 rest atom dangling bonds. The energy zero is the top of the valence band. (b) Two-dimensional Brillouin zone showing the directions Γ–Q, Q–P and P–Γ.

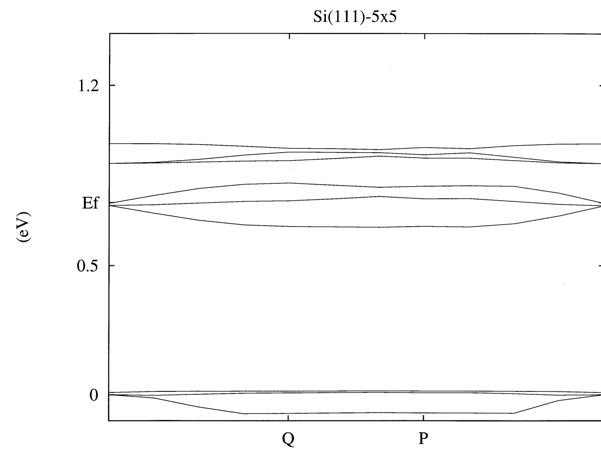

Fig. 6. LDA surface bands corresponding to the Si(111)-(5 × 5) reconstruction. The six bands around E_F are related to the six adatom dangling bonds, and the three bands ∼0.8 eV below E_F are associated with the corner hole atom and the two rest atoms dangling bonds. The energy zero is the top of the valence band. The directions Γ–Q, Q–P and P–Γ of the two-dimensional Brillouin zone are shown in Fig. 5(b).

It is interesting to note that the Fermi level is located in the middle of the adatom surface bands, in such a way that we find, per unit cell, 12 electrons filling the rest atom bands, 2 electrons in the corner hole band, and 5 electrons only in the adatom dangling bonds. These 19 electrons correspond to the number of dangling bonds associated with the rest atoms (6), corner hole (1) and adatoms (12). Our results show that the surface rehybridization provided by the DAS model pushes down the rest atom and corner hole dangling bonds, filling completely these states. As a consequence, the 12 adatom dangling bonds in this reconstruction are partially filled by 5 electrons. These partially occupied adatom bands define the 2D electron gas, whose correlation effects we shall discuss below.

A similar analysis can be performed for the Si(111)-(5 × 5) reconstruction. In this case we have 9 dangling bonds per unit cell: 2 rest atoms, a corner hole and 6 adatom dangling bonds. Figure 6 shows its LDA surface bands,[10] where we find a bunch of 6 bands around E_f associated with the adatom dangling bonds, one band located around 0.8 eV below E_f associated with the corner hole, and two bands located around 0.7–0.8 eV below E_f associated with the rest atoms.[38] As in the 7 × 7 case, the Fermi level is in the middle of the adatom surface bands and defines the following filling numbers for the different dangling bonds: 2 electrons per unit cell fill the corner hole surface band, 4 electrons the rest atom bands, and 3 electrons the 6 adatom bands. Similarly to the 7 × 7 reconstruction, the partially occupied adatom bands define the system where correlation effects can be important, but in this case with a

different occupancy (6 dangling bond bands filled by 3 electrons, as opposed to the 12 bands occupied by 5 electrons found for the 7×7). These differences in the filling factor will have important consequences for the determination of the metallic or semiconducting character of these reconstructions.

In order to analyze correlation effects in the surface bands calculated above, we have to define in a first step the generalized Hubbard Hamiltonian which we associate with that band structure. Following the discussion presented in Sec. 2, we start with the effective Hamiltonian (4) and look for the parameters $E_\alpha + V_\alpha^{\mathrm{mb}}$ and $t_{\alpha\beta}$, which yield a good fitting to the LDA bands. The surface symmetry simplifies the procedure, as some of the effective energy levels and hopping parameters associated with the different adatoms are equivalent. Figure 7 shows a top view of the unit cell of the different Si(111) DAS reconstructions, where the black dots highlight the position of the adatoms whose dangling bonds define the 2D electron gas presenting important correlation effects (12 adatoms for the 7×7, and 6 adatoms for the 5×5 reconstruction).

The fitting to the LDA bands reveals that essentially only two hopping parameters, T and s (see Fig. 7), are needed to reproduce the adatom surface bands. The values of these hopping parameters are:

$$\mathrm{Si(111)\text{-}}(7 \times 7): T \approx -76\ \mathrm{meV}; s \approx 25\ \mathrm{meV}\,;$$
$$\mathrm{Si(111)\text{-}}(5 \times 5): T \approx -70\ \mathrm{meV}; s \approx 21\ \mathrm{meV}\,.$$

The application of Eq. (12) to several "restricted" LDA calculations with different filling factors for the adatom bands provides a set of equations that can be used to calculate E_α, U_α and $J_{\alpha\beta}$, as discussed in Sec. 2. As already pointed out, there is always at least one parameter that still remains undetermined by the set of equations (12). In the case of the DAS reconstructions, we have chosen to obtain $J_{\alpha\beta}$ by means of an electrostatic model that approximates the adatom dangling bond charges by a point charge located ≈1.2 Å above a semi-infinite medium (with the bulk dielectric constant of Si, 11.9) simulating the Si crystal. Then restricted LDA calculations are used to calculate U_α, which appears to be almost constant for the different dangling bonds.

From these calculations we obtain (see Ref. 9 for details of the procedure) the following parameters for the 7×7 2D Hamiltonian [groups of atoms (1, 2, 3), (4, 5, 6), (7, 8, 9) and (10, 11, 12) in Fig. 7, which are equivalent by symmetry, are called r_1, r_2, d_1 and

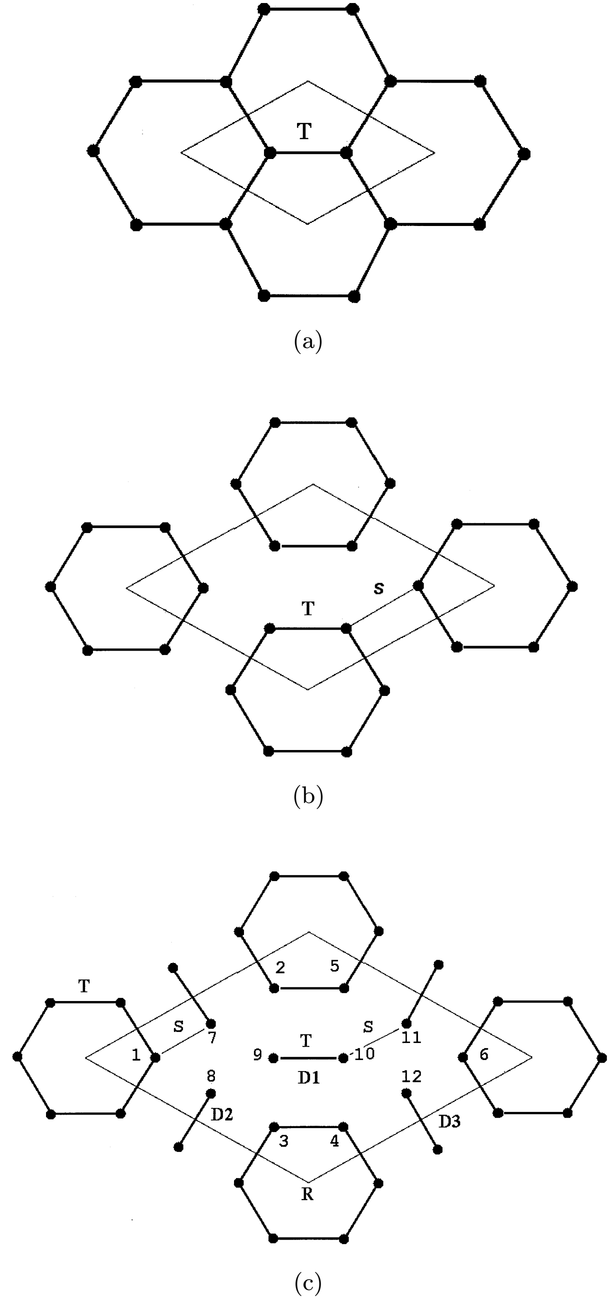

Fig. 7. Schematic representation of the adatom geometry and interactions: (a) Si(111)-(3×3), (b) Si(111)-(5×5) and (c) Si(111)-(7×7). The thick lines connecting adatoms represent the large hopping interactions, T, and the thin lines interactions s (for clarity, only a few s interactions are shown). The unit cell border is also shown.

d_2, respectively]:

$$E_{d_1} - E_{d_2} = -42 \text{ meV}\,;$$

$$E_{r_1} - E_{r_2} = -33 \text{ meV}\,;$$

$$E_d - E_r = 260 \text{ meV}\,;$$

$$U = 1.1 \text{ eV}\,;$$

where $E_d = (E_{d_1} + E_{d_2})/2$ and $E_r = (E_{r_1} + E_{r_2})/2$. From our electrostatic model J ranges from 386 meV for the nn interaction to zero.

The 5×5 reconstruction is analyzed in a similar way,[10] yielding the following parameters: $E_f - E_u = -108$ meV (E_f and E_u are the two levels associated with the atoms of the faulted and unfaulted sides of the unit cell), $U = 1.5$ eV, and values of J as in the 7×7 case.

3.1.2. *Correlation effects, metal–insulator transition*

We turn our attention to analyzing the electronic properties of the generalized Hubbard Hamiltonian [Eq. (1)] defined by the parameters given above.

3.1.2.1. Si(111)-(7 × 7)

Although we could apply to this case the general analysis presented in Sec. 2, we have found it more convenient to use a different approach that appears to be well suited to the particular Hamiltonian of this surface.[9] The crucial point in solving this case is to realize that the hopping integral t is substantially larger than s (see Fig. 7). This allows us to take $s = 0$ in the first step, and to include it later in the solution of that simplified Hamiltonian.

For $s = 0$, the structures having a hexagonal ring or a dimer geometry (Fig. 7) decouple from each other, and the system can be analyzed exactly. The solution of this Hamiltonian shows that the ground state corresponds to a configuration for which three electrons are localized in the hexagonal rings and the other two in the dimers. Specifying different configurations as $|N_R, N_1, N_2, N_3\rangle$, where N_R and N_i are the number of electrons in the ring and the different dimers (see Fig. 7), the ground state is $|3, 1, 1, 0\rangle$. The next most stable configuration corresponds to $|2, 1, 1, 1\rangle$ (its energy being 95 meV) and $|4, 1, 0, 0\rangle$ (with 125 meV). This shows that the system has the following neutral excitations:

$$|3, 1, 1, 0\rangle \to |2, 1, 1, 1\rangle\,,$$

$$|3, 1, 1, 0\rangle \to |4, 1, 0, 0\rangle\,,$$

corresponding to exciting one electron from the hexagonal ring to the dimer (95 meV), and one electron from a dimer to the hexagonal ring (125 meV), respectively. This solution also shows a threefold degeneracy for the ground state, corresponding to the states

$$|3, 1, 1, 0\rangle\,; \quad |3, 1, 0, 1\rangle\,; \quad |3, 0, 1, 1\rangle\,.$$

The main effect of a finite hopping s is to connect the threefold degenerate configurations. Notice that this corresponds to having three electrons frozen in the hexagonal ring structures, allowing the other two electrons to jump between dimers. This effect is going to create a metallic surface band. Figure 8 shows the local density of states (LDOS) for the ring and the dimers, as obtained from this solution: for $s = 0$ we obtain for the rings the LDOS of an isolated hexagonal ring filled with three electrons; for the dimers and $s = 0$, the ground state is defined by three sites (one site per dimer) filled by two electrons. Including the effect of s broadens the LDOS of the dimers and creates the metallic band, ≈100 meV width, located around E_F. In the case of the rings, as the electronic structure appearing around E_F is

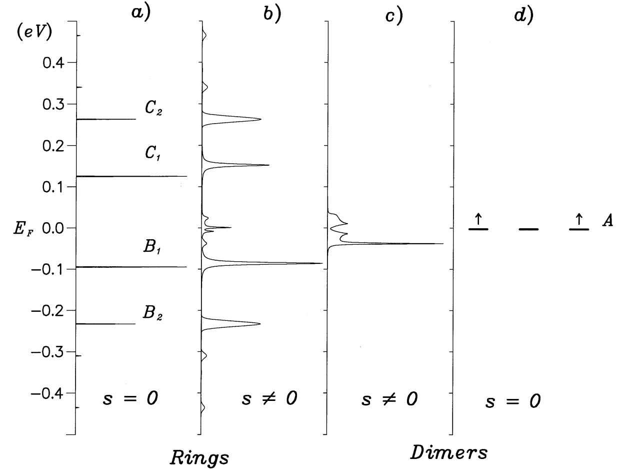

Fig. 8. Local density of states for the hexagonal ring and the dimers of the Si(111)-(7 × 7) surface, for $s = 0$ and $s \neq 0$. This density of states has been obtained using a spinless Hamiltonian and, therefore, the empty states should have twice the weight shown in the figure (see text).

practically decoupled from the dimer band, one can expect, in a first approximation, no major changes in the electronic structure when taking $s \neq 0$ except for a broadening of the peaks. There is, however, an interesting effect due to the charge fluctuations of the last occupied and first unoccupied state on the rings and the metallic DOS around E_F,[9] which leads to the appearance of a narrow Kondo-like peak (a few meV in width) at E_F (see Fig. 8).

It is worth commenting that the correlation effects of the metallic band associated with the two electrons filling three dimers have been analyzed approximately via an effective spinless Hamiltonian given by

$$\hat{H}_D = \sum_i E_d \hat{n}_i + \sum_{\text{nn}} s' \hat{d}_i^+ \hat{d}_i + \frac{1}{2} J^D \sum_{\text{nn}} \hat{n}_i \hat{n}_j \,, \quad (35)$$

where $s' = s/2 = 12$ meV defines the hopping integral between nn dimers and $J^D = 80$ meV their Coulomb interaction.

In this Hamiltonian, the on-site Coulomb interaction has been assumed to be infinity, and a possible metal–insulator transition might be driven by J^D. For $J^D/s' > 12$, electrons get frozen on the lattice sites, and the system behaves as insulating. We find, however, that $J^D/s' \approx 6$, and expect the 7×7 reconstruction to be metallic, with the LDOS shown in Fig. 7.

Note that the total density of filled states for the rings and the dimers is 3 and 2, respectively, while for the empty states we find, close to E_f, six states from the rings and two from the dimers (instead of three and one) due to the spin degeneracy (see the discussion on the spinless Hamiltonian at the end of Sec. 2).

We complete this section by mentioning that these results seem to be in reasonable agreement[9] with the experimental evidence provided by photoemission,[39] STM[40] and EELS.[5] For instance, STM conductances show a smaller occupied DOS for the dimer atoms than for the ring adatoms. Also, photoemission shows a peak that we associate with the DOS of the rings.[9]

3.1.2.2. Si(111)-(5×5)

This surface can also be analyzed using arguments similar to the ones presented above.[10] For the corresponding generalized Hubbard Hamiltonian, t is

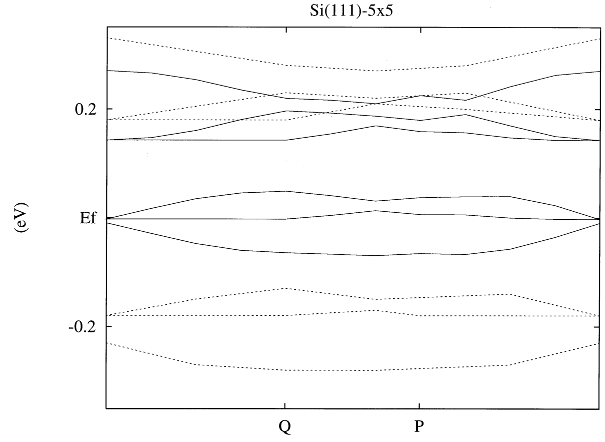

Fig. 9. LDA surface bands (solid lines) and correlated surface bands (dashed lines) around E_F for the Si(111)-(5×5) surface. The correlated surface bands below E_F are simply degenerate and each band contains only one electron per unit cell; above E_F each correlated surface band presents a total weight of two electrons per unit cell. The directions Γ–Q, Q–P and P–Γ of the two-dimensional Brillouin zone are shown in Fig. 5(b).

also much larger than s and we analyze correlation effects taking $s = 0$, in a first step. It is interesting to note that, in this limit, the system decouples only in hexagonal rings, each having three electrons, very much like in the 7×7 reconstruction. These isolated hexagonal rings can be analyzed solving exactly their finite Hamiltonian: their DOS shows, around E_F, three electrons and six holes, the same as for the results shown in Fig. 8 for the 7×7 [case (a): rings and $s = 0$]. In a further step, s is taken different from zero and the surface bands are calculated perturbatively. Figure 9 compares these correlated surface bands with the LDA ones.[37,10] Although the two calculations are similar (with a larger energy gap between the three lower and three higher bands in the correlated case), the main difference appears in the number of electrons associated with each band: in the correlated case, and due to the large U appearing in the generalized Hubbard Hamiltonian, the new bands below E_F in Fig. 9 are simply degenerate; this is the reason why the Fermi level is now located in an energy gap, and the system appears as semiconducting.[41]

It is also interesting to look at this problem as the solution of the generalized Hubbard Hamiltonian [Eq. (1)], where all the sites are practically equivalent (neglecting the energy difference between the faulted/unfaulted sides of the unit cell), and

the number of electrons is one every two sites, corresponding to a quarter-filling band. As commented in Sec. 2, in this system the metal–insulator transition could not be driven only by U; in our particular case, U is very large (larger than 1 eV) and, practically, we can assume it to be infinity. In spite of it, electrons can propagate along the crystal jumping to empty sites unless the off-site Coulomb interaction or the band structure conspires to prevent it.

In order to understand why the 5×5 is semiconducting, we can think of this 2D system (for U very large) as a spinless Hamiltonian. In this approximation, the electronic bands would appear as the LDA ones but only with a single electron occupancy. This explains the similarity between the LDA and our correlated bands; at the same time, it shows that our more detailed solution includes effects associated with the intersite interactions, $J_{\alpha\beta}$, that enhance the energy gap between the empty and the occupied bands. Thus, we conclude that the semiconducting behavior of the Si(5×5) reconstruction is due to both band structure and intersite Coulomb interaction effects.

3.1.2.3. Si(111)-(3×3)

Although this reconstruction has not yet been analyzed explicitly, we can deduce some of its general electronic properties using the results from the previous DAS reconstructions. The similarities of this case to the 7×7 and the 5×5 surfaces suggest that a Hamiltonian with parameters obtained by averaging the two other cases would be reliable for the purpose of our study. The surface unit cell of the 3×3 reconstruction has only two adatoms and a corner hole atom (see Fig. 7). From the previous calculations one can expect to have a surface band — associated with the corner hole — located around 0.8 eV below E_f; then the 2D electron gas is defined by the two adatoms dangling bonds filled only by one electron (quarter-filling band case). Averaging the results for the 7×7 and the 5×5 yields the parameters

$$E_f - E_u = -75 \text{ meV},$$
$$U = 1.2 \text{ eV},$$
$$t = -70 \text{ meV},$$

and the same values for J as in the 7×7 and the 5×5 reconstructions. We have checked that small changes of these parameters do not introduce substantial modifications in our conclusions.[9]

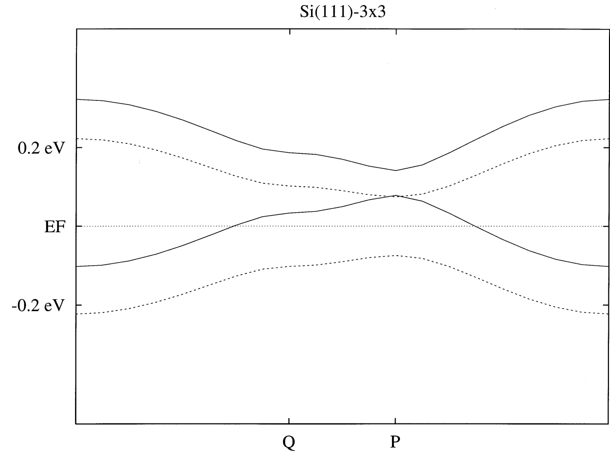

Fig. 10. Solid lines: surface bands around E_F obtained using an LD solution for the generalized Hubbard Hamiltonian for the Si(111)-(3×3) reconstruction. Dashed lines: correlated surface bands. Below E_F, each correlated surface band accommodates only one electron per unit cell, while above E_F each correlated surface band presents a total weight of two electrons per unit cell. The directions Γ–Q, Q–P and P–Γ of the two-dimensional Brillouin zone are shown in Fig. 5(b).

Figure 10 shows the bands calculated using an LD solution for the generalized Hubbard Hamiltonian. In this case, there is one electron per unit cell and the Fermi level is located in the middle of the lower band.

We analyze many-body effects assuming U very large, and introducing a spinless Hamiltonian with the parameters given above. Figure 10 also shows the bands for this Hamiltonian (dotted lines). Here, each band is occupied by a single electron and the Fermi energy appears in the energy gap yielding a semiconducting behavior for this reconstruction (as commented above, a more appropriate solution allows for a double occupancy of the empty band).

A word of caution is in order here, because this discussion depends very much on having assumed that one has only first neighbors interactions in the lattice. Including second (and further) neighbors interactions may modify the previous conclusion about the semiconducting behavior of this surface, because these interactions may introduce some overlap between the bands shown in Fig. 10. However, it should be kept in mind that the semiconducting behavior of this surface is mainly due to the difference in

energy between the dangling bonds associated with the faulted and the unfaulted sides of the 3×3 reconstruction. A definitive conclusion on the behavior of this reconstruction needs a full calculation.

3.2. *Si-rich SiC(111)-($\sqrt{3}\times\sqrt{3}$) and -(3×3) reconstructions*

SiC(111) surfaces, associated with either SiC(0001) or β-SiC crystals, present very similar reconstructions.[43] We shall discuss in this subsection, embodying all these different cases, the SiC(111) surfaces and the correlation effects that have been associated with the Si-rich $\sqrt{3}\times\sqrt{3}$ and 3×3 reconstructions.

Figure 11 shows the surface geometry of the $\sqrt{3}\times\sqrt{3}$ case. Si–C bilayers define the bulk, and the Si adlayer forming the $\sqrt{3}\times\sqrt{3}$ reconstruction is shown in the top and side views. Different theoretical and experimental groups[43–45] have identified the Si adsorption site as a T_4 position, on a threefold-coordinated site on top of the C atoms of the first bilayer.

It is interesting to note that each Si in the new adlayer forms three bonds with the Si atoms underneath. With this $\sqrt{3}\times\sqrt{3}$ structure, all the Si atoms of the last Si–C bilayer form four bonds with neighboring atoms, and the unsaturated dangling bonds of this reconstruction are associated only with the adlayer Si atoms.

Figure 12 shows the surface geometry of the 3×3 reconstruction as recently discovered by Starke *et al.*[46] This is a much more complicated structure, with the Si atoms of the last bilayer presenting a lateral relaxation. On top of this relaxed surface, there appears a Si adatom cluster of four atoms per unit cell, with three of them bonded to the relaxed Si surface and with the topmost one bonded to these three lower atoms of the cluster. It is important to note that with this structure, all the atoms (except the

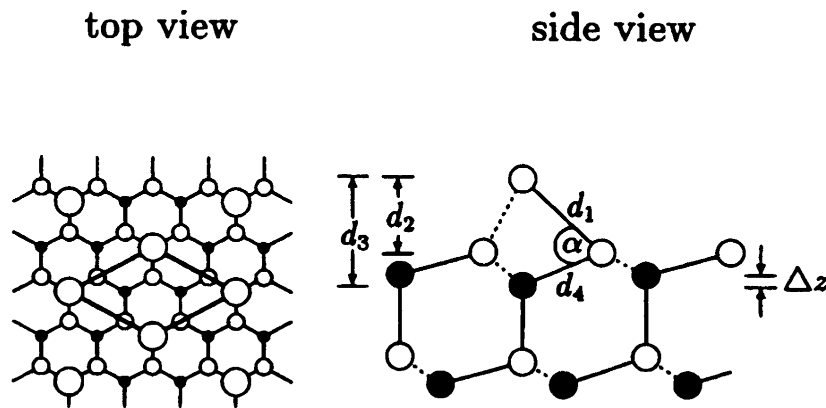

Fig. 11. Surface geometry of the SiC(111)-($\sqrt{3}\times\sqrt{3}$) reconstruction. (a) Top view; (b) side view.

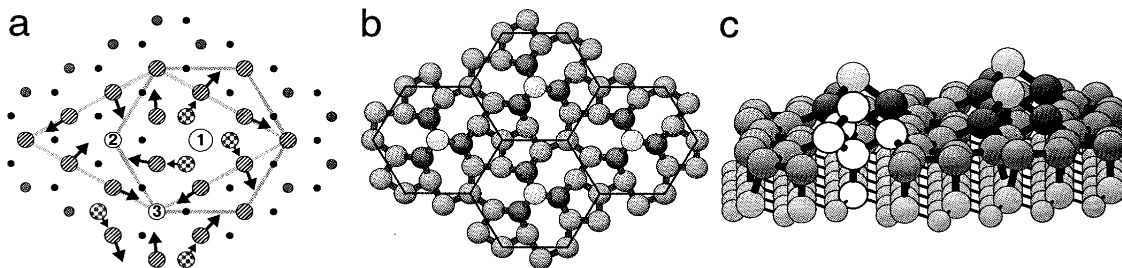

Fig. 12. The SiC(111)-(3×3) structure. (a) Lateral relaxation within the Si adlayer and the trimer supporting the adatom; (b) ball-and-stick model of the Si relaxation; (c) 3D view of the final structure.[46] Only the topmost Si atom has an unsaturated dangling bond (after Ref. 46).

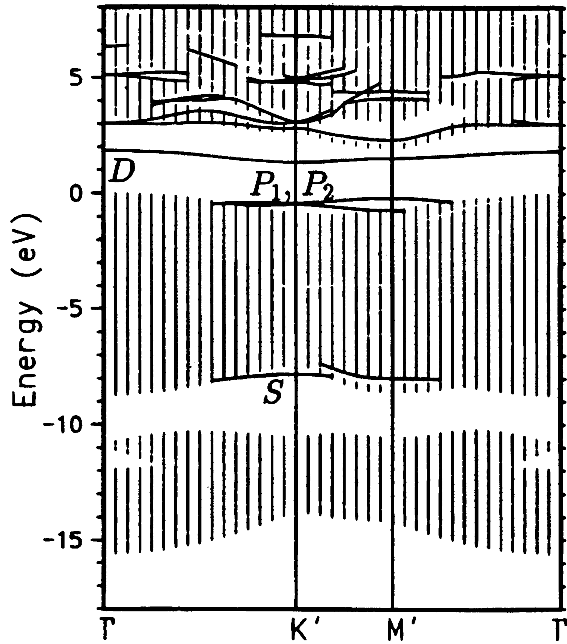

Fig. 13. Surface band structure of the Si-rich SiC(111)-($\sqrt{3} \times \sqrt{3}$) (after Ref. 43). The surface band associated with the half-occupied dangling bond of this reconstruction is located around 1.8 eV above the valence band top ($E = 0$). In this surface, $U^{\text{eff}}/W \simeq 5$, and the surface band would be split into two bands located around $\pm U^{\text{eff}}/2$ w.r.t. the initial Fermi level, located in the middle of the surface band.

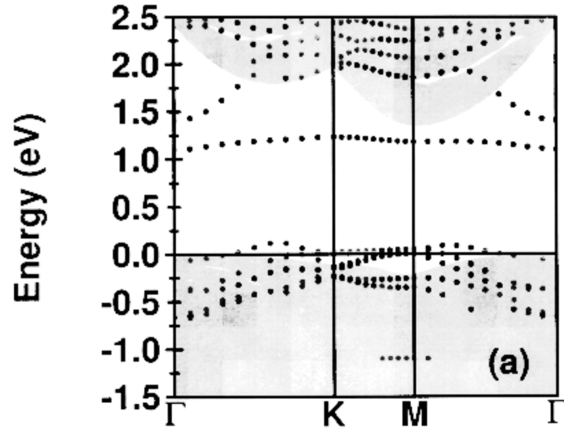

Fig. 14. Surface band structure of the Si-rich SiC(111)-(3×3) surface (after Ref. 46). The half-occupied surface band is located around 1.2 eV above the valence band top ($E = 0$). In this case, $U^{\text{eff}}/W \simeq 10$, and the surface band would be split into two bands located around ($\pm U^{\text{eff}}/2$) w.r.t. the initial Fermi energy.

topmost one) present a fourfold coordination with their bonds perfectly saturated. This shows that, in this geometry, there is only a nonsaturated dangling bond associated with the Si topmost surface atom.

3.2.1. *Local density calculations; surface bands and Hubbard Hamiltonian*

Different groups have analyzed, using an LD approximation, the electronic properties of the SiC(111)-($\sqrt{3} \times \sqrt{3}$) and -(3×3) surfaces.[7,43,44,8]

Figure 13 shows the surface band structure of the Si-rich SiC(111)-($\sqrt{3} \times \sqrt{3}$) reconstruction as calculated by Pollman and collaborators.[43] The important point, regarding our discussion of correlated surface bands, is that the Fermi level is in the middle of the surface band associated with the Si dangling bonds. This band is half-occupied, as corresponds to the electron that fills the dangling bonds.

Notice that the surface band is very narrow, with a width of only $\approx$0.3 eV, and that a restricted LDA calculation[7] yields $U^{\text{eff}} \approx 1.5$ eV. Correlation effects in this band can be analyzed using a restricted Hubbard Hamiltonian, where all the Coulomb interactions are included in U^{eff}. The discussion in Sec. 2 has shown that if U^{eff}/W is much larger than 1, we can expect the 2D electron gas to show a metal–insulator transition. For our system $U^{\text{eff}}/W \approx 5$ and we are clearly in the insulating phase. As discussed in the example of Fig. 1, for $U^{\text{eff}}/W \gg 1$, the band is split into two bands located around $\pm U^{\text{eff}}/2$ w.r.t. the initial Fermi level, the two bands presenting a width of half the initial LDA band width. Northrup and Neugebauer[7] have found these results to be in good agreement with the angle-resolved photoemission data.[4]

Bechstedt and collaborators[46] have also analyzed, using an LD approximation, the surface band structure of the Si-rich SiC(111)-(3×3) surface. Figure 14 shows their results, with a half-occupied surface band located around 1.2 eV above the valence band top. This band, associated with the dangling bond of the topmost Si atom, has only a bandwidth of 0.1 eV. This very small value is due to the large distance (see Fig. 12) between those dangling bonds. Bechstedt *et al.*[8] have estimated U^{eff} to be around 1 eV, 10 times the surface band width. We conclude that this surface band should also present strong correlation effects and would be split into two bands, very much like the case of the $\sqrt{3} \times \sqrt{3}$ reconstruction.

We conclude this section with the following comments:

(a) The surface bands associated with the Si-rich SiC(111)-($\sqrt{3} \times \sqrt{3}$) or -(3×3) reconstructions present important correlation effects and a *Hubbard–Mott* metal–insulator transition. In these cases, only U^{eff} is the driving mechanism for the phase transition.
(b) The surface bands associated with the Si(111)-(7×7), -(5×5) and -(3×3) reconstructions show a much richer variety. The reason is that the surface bands associated with the corner hole and/or the rest atoms are fully occupied. Then, the partially filled adatom bands present occupancies between 5/24 and 1/4; for these occupancies one has to resort to detailed calculations to analyze the correlation effects associated with these states. In view of the charge transfer appearing in these Si(111) reconstructions, we can say that — when it is present — the metal–insulator transition has a *charge transfer* character.

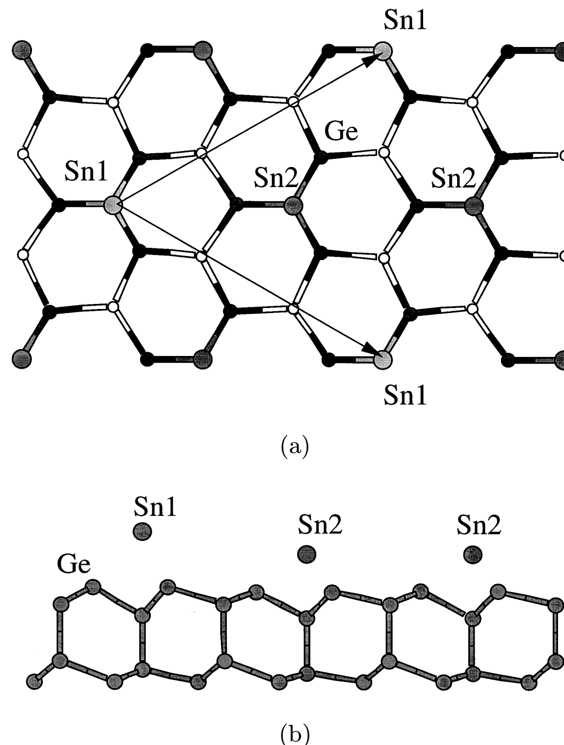

Fig. 15. (a) Top view and (b) side view of the Sn/Ge(111)-(3×3) reconstruction. In this surface, one Sn atom per unit cell is displaced upwards by 0.24 Å, and the other two Sn atoms are displaced downwards by 0.12 Å w.r.t. the Sn layer of the ideal $\sqrt{3} \times \sqrt{3}$ reconstruction.

4. Interfaces

In this section we shall analyze different semiconductor interfaces where electron correlation effects have been found to be important. The first case we discuss is the Sn/Ge(111) interface, which shows, at low temperature, a 3×3 reconstruction. This system — and the Pb/Ge(111) case — presents a surface phase transition from the room temperature $\alpha(\sqrt{3}\times\sqrt{3})$-$R30°$ phase to the mentioned 3×3 structure at around 200–250 K.[3,14] This transition has recently been explained as a dynamical fluctuation between two positions of the Sn atoms adsorbed on the Ge(111): at low temperature, this fluctuation is stabilized and the interface shows a 3×3 reconstruction, with two inequivalent Sn atoms located at different heights on the Ge surface.[47] In this paper we analyze this 3×3 reconstruction, whose geometry[48,49] is shown in Fig. 15, and point out some striking similarities it has to the Si(111)-(3×3) reconstruction discussed above.

As a second example where important correlation effects appear at semiconductor interfaces, we analyze the case of alkali metals (AM) deposited on semiconductors. We consider two cases — one is the AM/GaAs(110) interface. This is an important system from the point of view of the metal–semiconductor junction. In this paper, we only discuss how metallization appears when alkali atoms are deposited on GaAs(110) (readers interested in the more general problem of the Schottky barrier formation are referred to Ref. 13). The other case we discuss is the K/Si(111)-($\sqrt{3} \times \sqrt{3}$)-B interface, which has recently been shown to present a Mott-insulating ground state.[2]

4.1. *Sn/Ge(111)-(3 × 3) reconstruction*

This reconstruction has been analyzed theoretically using a first principles molecular dynamics technique.[47] In this approach, a local orbital self-consistent LDA method is used to obtain first principles atomic forces efficiently. The geometry found for the 3×3 reconstruction (see Fig. 15) shows one Sn atom per unit cell displaced upwards 0.24 Å and

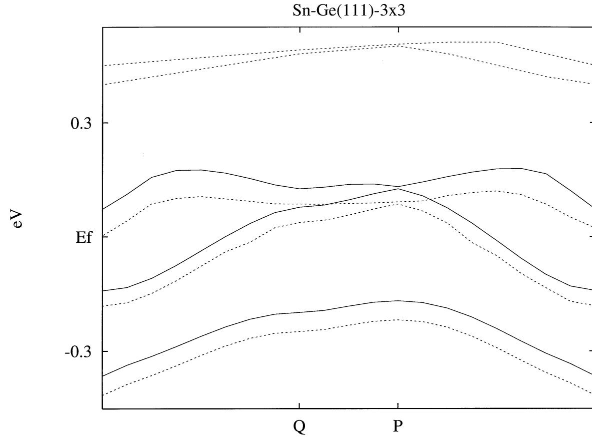

Fig. 16. LDA surface bands (solid lines) and correlated surface bands (dotted lines) of the Sn/Ge(111)-(3×3) surface. The lower surface band is doubly occupied, while the two surface bands around E_F accommodate only one electron; the total weight of each of these surface bands is 1.5 electrons (spin included). The surface bands ~ 0.4 eV above E_F present the remaining total weight of one electron (0.5 electrons each band). The directions Γ–Q, Q–P and P–Γ of the two-dimensional Brillouin zone are shown in Fig. 5(b).

the other two Sn atoms displaced downwards 0.12 Å w.r.t. the Sn layer of the $\sqrt{3} \times \sqrt{3}$ symmetry. In Fig. 16 (solid lines) we show the calculated LDA bands for the 3×3 reconstruction. One can understand the energy position of the surface bands in terms of the reconstructed geometry. For the Sn atom displaced upwards, rehybridization causes its dangling bond to have a more s-like character and a corresponding lower energy (more binding energy). The lower surface band in Fig. 16 is associated with that atom and it is doubly occupied. On the other hand, the other two surface bands — located around E_F — are associated with the two dangling bonds of the Sn atoms moving downwards. In these atoms, the rehybridization due to the new reconstruction tends to shift their dangling bond levels towards higher energies.

It is interesting to compare this reconstructed surface with the Si(111)-(3 × 3). In both cases we find similar geometries associated with the atoms whose surface bands are located around the Fermi energy, and we also find the same one-quarter band filling. In the Si(111)-(3×3) reconstruction, the lower fully occupied band is associated with the corner hole atom, while in the Sn/Ge(111)-(3 × 3) interface we find a similar doubly occupied surface band associated with the Sn atom that has relaxed towards the vacuum side. The main difference between the band structure of these two sytems close to E_F can be related to the energy levels of the two partially occupied dangling bonds, which in the Sn/Ge(111) case are practically the same, while in the Si(111)-(3 × 3) case there is an energy difference of around 70 meV due to the inequivalence between the faulted and unfaulted sides of the surface. Note that the two surface bands around E_F for the Sn/Ge(111) case overlap in energy and show a metallic character. This is in contrast to the semiconducting behavior of the surface bands found for the Si(111)-(3 × 3) and it is the result of having two equivalent Sn atoms in the Sn/Ge(111)-(3 × 3) reconstruction.

In order to define the parameters U and J associated with the generalized Hubbard Hamiltonian for this reconstruction, we have also used a restricted LDA calculation and have assumed that electrons in different dangling bonds interact with each other like point charges located in front of a semiconductor surface. This approach yields $U \approx 0.9$ eV and values of J ranging between 0.35 eV (for nn charges) and zero (for long distant charges).

In a further step, we have calculated correlation effects on the surface bands by introducing the local self-energy defined in Sec. 2, and treating the off-site Coulomb interaction, J, in a mean field approximation. Dashed lines in Fig. 16 show the correlated bands calculated in this way. Important points about the results are:

(a) The doubly occupied surface band located around 0.3 eV below E_F is barely modified by correlation effects, keeping its total weight of two electrons per unit cell.

(b) The two surface bands located around E_F are split into two discontinued pieces. The one around E_F is still similar to the initial LDA bands although, instead of having a total weight of four electrons (for two bands) per unit cell, it has now a total weight of $4 \times \frac{3}{4} = 3$ electrons. On the other hand, we find a new structure, around 0.5 eV (this is the value of $U^{\text{eff}} \approx U - J$, with J the nn Coulomb interaction) above E_F, with a total weight of $4 \times \frac{1}{4} = 1$ electron per unit cell. These results should be compared with our discussion of Fig. 2, and they show that correlation

effects reduce the total density of states around E_F by a factor of $\frac{3}{4}$ for a quarter-filling band.

(c) Finally, we note that, in spite of these important correlation effects, the system is still metallic, in contrast with what we found for the Si(111)-(3×3) reconstruction. In relation to Fig. 2, we should also say that in this surface J^{eff} is not large enough to drive a metal–insulator transition as shown in Fig. 2(c).

In conclusion, correlation effects for this interface are relevant but they do not change too much the surface state band structure associated with the bands located around or below E_F. A new structure appears, however, in the density of states located 0.4 eV above E_F. It is worth commenting that the two bands located below E_F have been observed with photoemission,[47,50] yielding a strong support to the results presented for the Sn/Ge(111)-(3×3) interface.

4.2. *Alkali atoms on GaAs(110)*

The adsorption of alkali atoms on GaAs(110) has been a subject of great interest for understanding the early stages of the Schottky barrier formation.[51] The advantage of using alkali atoms is that they do not diffuse into the semiconductor crystal and that they tend to form a flat monolayer for an appropriate coverage.

Our discussion in this paper about this interface will be limited to analyzing the surface geometry, the surface bands and the correlation effects appearing for alkali metal coverages of less than or around a monolayer. A more complete discussion on this problem can be found in Ref. 13.

The adsorption of Na, K or Cs on GaAs(110) has been analyzed by several groups.[12,51,52] In the limit of very low coverages, alkali atoms tend to adsorb on the Ga dangling bonds as shown schematically in Fig. 17, where a top view of the GaAs(110) surface is shown, indicating the preferential sites for atomic Na or K adsorption.[53,54] For increasing coverages alkali metal atoms tend to form linear chains and/or small islands before reaching the physical coverage limit of a monolayer.[52]

Correlation effects, in this coverage limit of a physical monolayer, have been analyzed theoretically by assuming that alkali atoms (Na or K) saturate all the Ga dangling bonds of the GaAs(110) surface

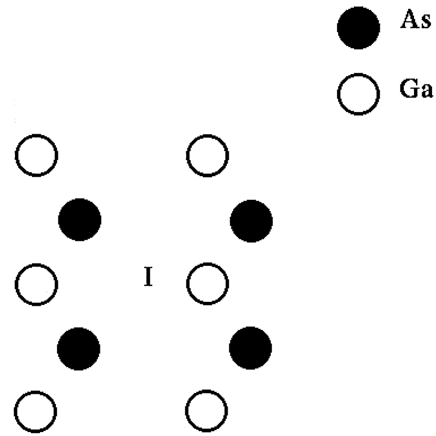

Fig. 17. Schematic top view of the GaAs(110) surface indicating the adsorption site, I (Ga dangling bond), of the alkali atoms.

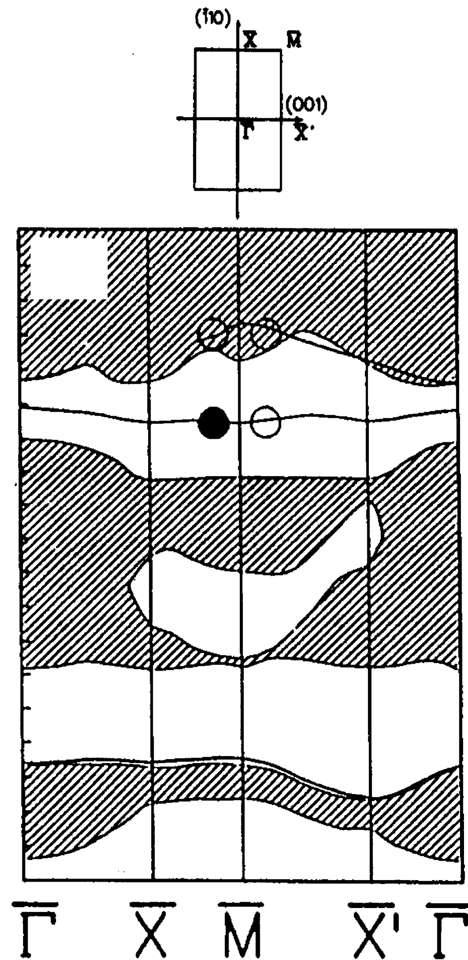

Fig. 18. Band structure of the Na/GaAs(110) interface, for a coverage of $\theta = 1/2$ (after Ref. 55). For this coverage, one alkali atom saturates each Ga dangling bond.

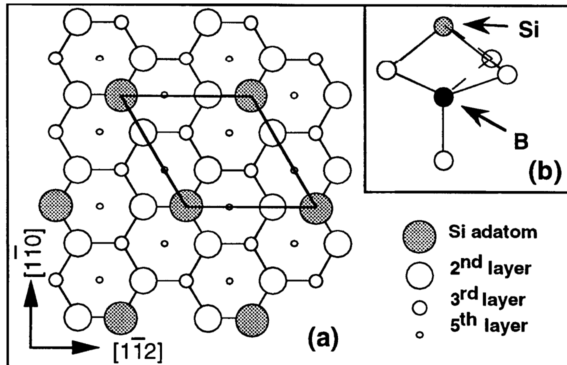

Fig. 19. (a) Top view and (b) side view of the K/Si(111)-($\sqrt{3} \times \sqrt{3}$)-B interface. The B atoms are located substitutionally in the second layer of the crystal.

(this is nominally a coverage of $\Theta = \frac{1}{2}$).[54,13] Figure 19 shows the electronic surface band structure for the Na/GaAs(110) interface as calculated by Hebenstreit *et al.*[55] for this coverage. This, as well as other calculations for K,[53] shows that the effect of the alkali layer is to create a half-occupied surface band located in the middle of the semiconductor energy gap. As the surface band width is small, around 0.5–0.7 eV, we can expect to find important correlation effects in the 2D electron gas associated with that band.

Restricted LDA calculations[6,54] for the Na and K/GaAs(110) interfaces have given values of $U^{\text{eff}} =$ 1.5 and 0.6 eV respectively. Other estimates for K have yielded $U^{\text{eff}} = 1.2$ eV.[56] In view of these uncertainties, we can only say that U^{eff} is around 0.9 eV, a value that may have an error of ± 0.3 eV.

Using this value of U^{eff}, and the surface band structure shown in Fig. 17, one can follow the analysis of Sec. 2 and the results shown in Fig. 1 to decide on the existence of a Mott transition in this interface. For Na and K, we find that $U^{\text{eff}}/W \approx 1.8$ and 1.5 for $\Theta = \frac{1}{2}$, respectively. This suggests that the monolayer of Na is insulating and that its K counterpart is around the metal–insulator transition point. Considering the uncertainty in the value of U^{eff}, one should, however, take these results with some care.

Notice that for $\Theta < \frac{1}{2}$, the width of the surface band is going to decrease and U^{eff} to increase (because of the smaller screening due to the nearest neighbors). This indicates that U^{eff}/W increases for smaller coverages, suggesting that the system is going to have a Mott transition not far from the $\frac{1}{2}$ nominal coverage.

These results have extreme importance when one analyzes the formation of a metal–semiconductor interface in the limit of low coverage. The point to note is that for very low coverages ($\Theta < \frac{1}{2}$), the metal layer deposited on the semiconductor is not yet metallic and that the interface Fermi level can fluctuate in the semiconductor energy gap depending on the semiconductor doping. Only for coverages $\Theta > \frac{1}{2}$ does the metal layer become metallic and the interface Fermi level can be pinned by a finite density of states. At that moment the Schottky barrier is formed and we find a barrier height that practically corresponds to a fully developed interface.[13]

4.3. *K/Si(111)-($\sqrt{3} \times \sqrt{3}$)-B interface*

This is another example where correlation effects have been observed experimentally.[2] Figure 19 shows the geometry of the K/Si(111)-($\sqrt{3} \times \sqrt{3}$)-$R30°$-B interface. In this geometry, Si adatoms form a $\sqrt{3} \times \sqrt{3}$ lattice. The B atoms are located in substitutional sites in the second layer of the crystal, just below the Si adatoms, as shown in Fig. 19.

The important thing to note is that the B atoms (valence 3) take the electrons of the Si adatom dangling bonds, leaving empty the surface band associated with these dangling bonds.

When K is deposited on this surface, electrons are transferred from the alkali atoms to the empty dangling bonds, creating for a $\sqrt{3} \times \sqrt{3}$ lattice (with K forming a structure in registry with the initial one) a half-occupied surface band. As Weitering *et al.* have commented:[2] "This interface should be metallic according to band theory. Instead, the single particle excitation spectra show two prominent features near E_F, which are identified as the Hubbard bands of a 2D Hubbard system."

Figure 20 shows the photoemission and the inverse photoemission spectra for this system,[2] as a function of the K coverage, between $\Theta = 0$ and $\Theta = \frac{1}{3}$. From these curves, one can deduce that there is an effective intrasite Coulomb interaction, U^{eff}, of around 1.5 eV. This value is much larger than the bandwidth of the half-occupied surface band that is estimated by Weitering *et al.*[2] to be around 0.2 eV. We see that U^{eff}/W is around 7.5, much larger than 1–2, the value for which we can expect the system to present a metal–insulator transition, confirming

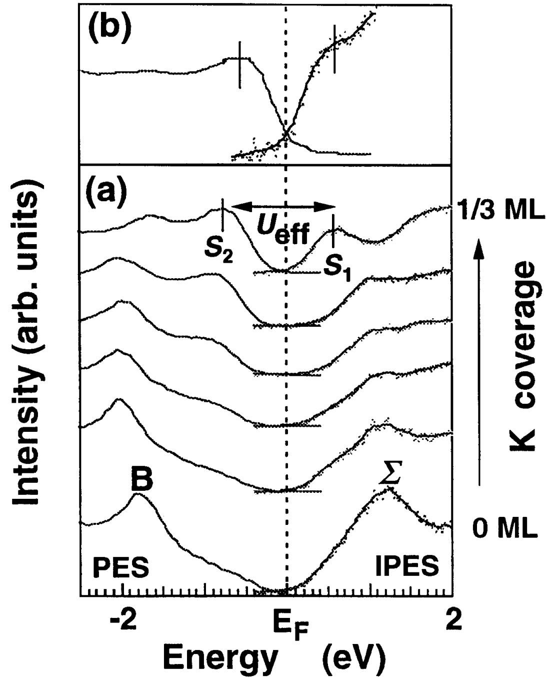

Fig. 20. Direct and inverse photoemission spectra of the K/Si(111)-($\sqrt{3} \times \sqrt{3}$)-B interface (after Ref. 2). U^{eff} is defined by the two peaks, S_2 and S_1, appearing in the direct and inverse photoemission spectra, respectively.

theoretically that this system presents a Mott-insulating ground state.

5. Conclusions

The analysis presented in this paper shows that many different surfaces and interfaces present important many-body effects that modify dramatically the one-electron picture yielded by an LDA calculation.

Several cases, including the Si-rich SiC(111)-($\sqrt{3} \times \sqrt{3}$) and -(3×3) reconstructions, the alkali atom – GaAs(110) interface and the K/Si(111)-($\sqrt{3} \times \sqrt{3}$)-B interface, can be classified as a Mott–Hubbard insulator system with a half-filled dangling bond surface band. These cases can be analyzed using a restricted Hubbard Hamiltonian, for which the main parameters characterizing the system are the effective intrasite Coulomb repulsion, U^{eff}, and the bandwith W. Typically, the systems analyzed [except the AM/GaAs(110) for a half-monolayer coverage] present values of U^{eff}/W much larger than 1, defining an insulating phase, and showing that the one-electron picture provided by the LDA calculations breaks down.

Other cases, like the Si(111)-(7×7), -(5×5) and -(3×3) reconstructions or the Sn/Ge(111)-(3×3) interface, are more complicated. In a sense, these are *charge transfer* systems where electrons near the Fermi energy are transferred from particular dangling bonds forming the surface bands to more localized levels. For instance, in the Si(111)-$[(2n+1) \times (2n+1)]$ reconstructions electrons from the adatom dangling bonds are transferred to the rest atoms and/or the corner hole dangling bonds. This defines a 2D electron gas with mean electron occupancies per dangling bond smaller than 1 (or 1/2 per spin). For example, in the Si(111)-(7×7) we find 5 electrons in 12 dangling bonds (defining a 5/24 occupancy per spin), in the Si(111)-(5×5) 3 electrons fill 6 dangling bonds (with a 1/4 occupancy), and in the Si(111)-(3×3) reconstruction 1 electron fills 2 dangling bonds (also with a 1/4 occupancy). It is interesting to note that the Sn/Ge(111)-(3×3) interface also shows a geometry similar to the one found in the Si(111)-(3×3) reconstruction, with 2 electrons filling the dangling bond of the Sn moving upwards. Then, the partially occupied surface bands correspond to having 1 electron filling 2 dangling bonds (with a 1/4 occupancy, as in previous examples).

The analysis of these charge transfer systems is more involved than that presented for the restricted Hubbard–Mott insulator and needs a specific discussion. Moving from the simpler cases to the more complicated ones, we mention first the Si(111)-(5×5) reconstruction where we find, basically, electrons almost localized in hexagonal structures. This yields an insulating phase due to the Coulomb interactions appearing in the hexagonal rings and also to the small hopping interactions between those structures. The Si(111)-(7×7) reconstruction presents some hexagonal surface structures similar to the ones found for the Si(111)-(5×5); our analysis shows that three electrons, out of the five filling the surface bands, get localized in those hexagonal rings. The other two electrons per unit cell can move along some "dimer" structures that appear intercalated among the rings. We find that these two electrons are responsible for the metallicity of the Si(111)-(7×7) reconstruction.

Finally, the Si(111)-(3×3) surface and the Sn/Ge(111)-(3×3) interface show similar band fillings but have different characters. The Si(111)-(3×3)

surface is found to be insulating, basically due to the difference between the faulted and unfaulted levels of the corresponding adatom dangling bonds. The Sn/Ge(111)-(3×3) interface appears, however, to be metallic. This is basically the result of having two equivalent dangling bonds per unit cell contributing to the formation of a metallic band in spite of the strong Coulomb repulsion between electrons.

We conclude that, at variance with the Mott–Hubbard insulator, the 2D charge transfer systems show a rich variety with either a semiconducting or a metallic character, depending as much on the surface geometry as on the electron–electron interaction.

Acknowledgments

We thank A. Martín-Rodero and A. Levy Yeyati for the many helpful discussions. This work was funded by the Spanish CICYT under contract No. PB97-0028.

References

1. N. J. Dinardo, T. Maeda Wong and E. W. Plummer, *Phys. Rev. Lett.* **65**, 2177 (1990).
2. H. H. Weitering, X. Shi, P. D. Johnson, J. Chon, N. J. Dinardo and K. Kempa, *Phys. Rev. Lett.* **78**, 1331 (1997).
3. J. Carpinelli, H. H. Weitering, E. W. Plummer and R. Stumpf, *Nature* **381**, 398 (1996); A. Goldoni and S. Modesti, *Phys. Rev. Lett.* **79**, 3266 (1997).
4. L. I. Johansson, F. Owman and P. Martensson, *Surf. Sci.* **360**, L478 (1996); J. M. Themlin, I. Forbeans, V. Langlais, H. Belkhir and J. M. Debever, *Europhys. Lett.* **39**, 61 (1997).
5. J. E. Demuth, B. N. J. Persson and A. J. Schell-Sorokin, *Phys. Rev. Lett.* **51**, 2214 (1983).
6. O. Pankratov and M. Scheffler, *Phys. Rev. Lett.* **70**, 351 (1993).
7. J. E. Northrup and J. Neugebauer, *Phys. Rev.* **B57**, R4231 (1998).
8. J. Furthmüller, F. Bechstedt, H. Hüsker, B. Schröter and W. Richter, *Phys. Rev.* **B58**, 13712 (1998).
9. J. Ortega, F. Flores and A. Levy Yeyati, *Phys. Rev.* **B58**, 4584 (1998).
10. J. Ortega, A. Levy Yeyati and F. Flores, *Appl. Surf. Sci.* **123/124**, 131 (1998).
11. G. Santoro, S. Sorella, F. Becca, S. Scandolo and E. Tosatti, Cond-Mat/9802014 (1998).
12. K. Stiles and A. Kahn, *Phys. Rev. Lett.* **60**, 440 (1988); K. Stiles, A. Kahn, D. Kilday and G. Margaritondo, *J. Vac. Sci. Technol.* **B5**, 987 (1987); W. E. Spicer, *Appl. Surf. Sci.* **41/42**, 1 (1989).
13. F. Flores, *Surf. Rev. Lett.* **2**, 513 (1995).
14. J. Carpinelli, H. H. Weitering and E. W. Plummer, *Phys. Rev. Lett.* **79**, 2859 (1997).
15. H. Eskes, M. B. J. Meinders and G. A. Zawatsky, *Phys. Rev. Lett.* **67**, 1035 (1991).
16. V. I. Anisimov, J. Zaanen and O. K. Andersen, *Phys. Rev.* **B44**, 943 (1991).
17. J. P. Perdew and A. Zunger, *Phys. Rev.* **B23**, 5048 (1981).
18. See for instance: W. Jones and N. H. March, *Theoretical Solid State Physics* (Wiley-Interscience, London, 1973); R. Micnas J. Ranninger and S. Robaszkiewicz, *Rev. Mod. Phys.* **62**, 113 (1990).
19. A. Georges, G. Kotliar, W. Krauth and M. J. Rozenberg, *Rev. Mod. Phys.* **68**, 13 (1996).
20. F. J. García-Vidal, J. Merino, R. Pérez, R. Rincón, J. Ortega and F. Flores, *Phys. Rev.* **B50**, 10537 (1994).
21. G. D. Mahan, *Many-Particle Physics* (Plenum, New York, 1981).
22. A. Levy Yeyati, A. Martín-Rodero, F. Flores, J. Ortega and R. Rincón, *Appl. Surf. Sci.* **104/105**, 248 (1996).
23. See for instance: D. Spanjaard and M. C. Desjonqueres, in *Interaction of Atoms and Molecules with Solid Surfaces*, eds. Bortolani *et al.* (Plenum, New York, 1990).
24. A. Martín-Rodero, F. Flores, M. Baldo and R. Pucci, *Solid State Commun.* **44**, 911 (1982).
25. H. Kajnater and G. Kotliar, *Phys. Rev. Lett.* **77**, 131 (1996); A. Levy Yeyati, A. Martín-Rodero and F. Flores, *Phys. Rev. Lett.* **71**, 2991 (1993).
26. M. Rozenberg, X. Y. Zhang and G. Kotliar, *Phys. Rev. Lett.* **69**, 1236 (1992).
27. J. A. White, *Phys. Rev.* **B45**, 1100 (1992).
28. F. Flores, A. Levy Yeyati, A. Martín-Rodero and J. Merino, *Phys. Low Dim. Struct.* **1**, 23 (1994).
29. R. E. Schlier and H. E. Fernsworth, *J. Chem. Phys.* **30**, 917 (1959).
30. R. S. Becker, J. A. Golovchenko, G. S. Higashi and B. S. Swartzentruber, *Phys. Rev. Lett.* **57**, 1020 (1986).
31. R. S. Becker, B. S. Swartzentruber, J. S. Vickers and T. Klitsner, *Phys. Rev.* **B39**, 1633 (1989).
32. K. Takayanagi, Y. Tanishiro, M. Takahashi and S. Takahashi, *Surf. Sci.* **164**, 367 (1985); *J. Vac. Sci. Technol.* **A3**, 1502 (1985).
33. A. A. Demkov, J. Ortega, O. F. Sankey and M. P. Grumbach, *Phys. Rev.* **B52**, 1618 (1995); O. F. Sankey and D. J. Niklewski, *Phys. Rev.* **B40**, 3979 (1989).
34. CETEP L. J. Clarke, I. Stich and M. C. Payne, *Comput. Phys. Commun.* **72**, 14 (1992).
35. R. I. Uhrberg, T. Kaurila and Y. C. Chao, *Phys. Rev.* **B58**, R1730 (1998).
36. F. Flores, A. Levy Yeyati and J. Ortega, *Surf. Rev. Lett.* **4**, 281 (1997).
37. R. Pérez, J. Ortega and F. Flores, to be published.

38. J. Ortega, F. Flores, R. Pérez and A. Levy Yeyati, *Prog. Surf. Sci.* **59**, 233 (1998).
39. F. J. Himpsel, D. E. Eastman, J. A. Knapp and K. C. Pandey, in *Proc. 14th Conf. on the Physics of Semiconductors*, ed. B. L. H. Wilson (Edinburgh, 1978); R. I. G. Uhrberg and G. V. Hansson, *Crit. Rev. Solid State Mater. Sci.* **17**, 133 (1991); M. E. Dávila, Ph.D. thesis (Universidad Autónoma de Madrid, 1996).
40. R. Wolkow and Ph. Avouris, *Phys. Rev. Lett.* **60**, 1049 (1988).
41. R. M. Feenstra and M. A. Lutz, *J. Vac. Sci. Technol.* **B9**, 716 (1991).
42. R. Kaplan, *Surf. Sci.* **215**, 11 (1989); L. Li, Y. Hasegawa, T. Sakurai and I. S. T. Tsong, *J. Appl. Phys.* **80**, 2524 (1996).
43. M. Sabisch, P. Krüger and J. Pollmann, *Phys. Rev.* **B55**, 10561 (1997).
44. J. E. Northrup and J. Neugebauer, *Phys. Rev.* **52**, 17001 (1995).
45. F. Owman and P. Martensson, *Surf. Sci.* **330**, L639 (1995).
46. U. Starke, J. Schardt, J. Bernhardt, M. Franke, K. Reuter, H. Wedler, K. Heinz, J. Furthmüller, P. Käckel and F. Bechstedt, *Phys. Rev. Lett.* **80**, 758 (1998).
47. J. Avila, A. Mascaraque, E. G. Michel, M. C. Asensio, G. LeLay, J. Ortega, R. Pérez and F. Flores, *Phys. Rev. Lett.* **82**, 442 (1999).
48. A. Mascaraque, J. Avila, E. G. Michel and M. C. Asensio, *Phys. Rev. Lett.*, in press.
49. J. Zhang, P. J. Rous, A. P. Baddorf and E. W. Plummer, to be published.
50. R. Uhrberg and T. Balasubramanian, *Phys. Rev. Lett.* **81**, 2108 (1998).
51. M. Prietsch, M. Danke, C. Laubschat and G. Kaindl, *Phys. Rev. Lett.* **60**, 436 (1988).
52. L. J. Whitman, J. A. Stroscio, R. A. Dragoset and R. J. Celotta, *Phys. Rev. Lett.* **66**, 1338 (1991).
53. J. Ortega and F. Flores, *Phys. Rev. Lett.* **63**, 2500 (1989).
54. F. Bechstedt and M. Scheffler, *Surf. Sci. Rep.* **18**, 145 (1993).
55. J. Hebenstreit, M. Heinemann and M. Scheffler, *Phys. Rev. Lett.* **67**, 1031 (1991).
56. F. Flores and J. Ortega, *Europhys. Lett.* **17**, 619 (1992).